Young Scientists Workshop 2004

SFB 484

INSTITUT für PHYSIK
UNIVERSITÄT AUGSBURG
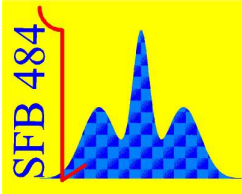
Book of Abstracts

Reimlingen

June 10-13, 2004

Contents

Program

10:00		Meeting at Augsburg station, platform 3 Nord
10:27		Leave from Augsburg station
11:33		Arrival at Nördlingen station, bus transfer to Reimlingen
12:30		Check-in at Bildungshaus St. Albert
13:00		Lunch
14:15	Krimmel, Eyert	Welcome
14:30 - 15:15	Götzfried	Hexagonal Perovskites and Related Structures
15:15 - 16:00	Laschinger	Magnetic Chains in $Ca_3Co_2O_6$
16:00 - 16:30		Coffee
16:30 - 17:15	Aliaga	Novel Algorithm for 3D Manganites
17:15 - 18:00	Fichtl	Dielectric Spectroscopy and its Application to Transition-Metal Chalcogenides
19:00		Dinner

08:00		Breakfast
09:00 - 09:45	Schrupp	Polaronic Physics of Magnetite
09:45 - 10:30	Leonov	Charge and Orbital Order in Fe_3O_4
10:30 - 11:00		Coffee
11:00 - 11:45	Schneider	Bipolaron Formation: A Comparison of the Hubbard-Holstein and the $E \otimes \beta$-Jahn-Teller-Hubbard Model
11:45 - 12:30	Mocanu	Finite Size Bosonization and Self-Consistent Harmonic Approximation
13:00		Lunch
Afternoon	*Trip to Nördlingen*	
19:00		Dinner
20:00 - 20:45	Eickerling	Occurence and Consequences of Charge Concentrations in Transition Metal Oxides
20:45 - 21:30	Körting	Interface-Mediated Pairing in Field Effect Devices

Saturday, June 12, 2004

08:00		Breakfast
09:00 - 09:45	Weber	The Grain Boundary Problem and its Possible Solution for Applications in High-T_c Superconductors
09:45 - 10:30	Lee	Quantum Phase Transitions in Models of Magnetic Impurities
10:30 - 11:00		Coffee
11:00 - 11:45	Sellier	Josephson Tunneling Through a Quantum Dot
11:45 - 12:30	Lobaskin	Crossover from Non-Equilibrium to Equilibrium Behavior in the Time-Dependent Kondo Model
13:00		Lunch
14:30 - 15:15	Schwingenschlögl	Electronic Structure of Vanadium Oxides
15:15 - 16:00	Keller	Realistic Modelling of Strongly Correlated Systems in LDA+DMFT
16:00 - 16:30		Coffee
16:30 - 17:15	Ren	The Self-Consistent LDA+DMFT Scheme in Wannier Representation
19:00		Dinner

Sunday, June 13, 2004

08:00		Breakfast
09:00 - 09:45	Rudolf	Optical Spectroscopy of Transition-Metal Oxides
09:45 - 10:30	Hoinkis	Mott Transition at the Surface of $1T$-$TaSe_2$ Studied by Angle-Resolved Photoemission
10:30 - 11:00		Coffee
11:00 - 11:30	Krimmel, Eyert	Closing remarks
12:00		Lunch
13:00		Bus transfer to Nördlingen station
14:15		Leave from Nördlingen station
15:29		Arrival at Augsburg

1 Thomas Götzfried: Hexagonal Perovskites and Related Structures

The perovskite family of oxides is perhaps the most studied group of oxides known [1]. The structure of the ideal ABO_3 perovskite with $Pm\overline{3}m$ symmetry can be described as a three-dimensional network built of corner-sharing BO_6 octahedra with the A cations occupying the large 12-fold coordinated cubo-octahedral cavities. What has generated and sustained the interest in this fascinating family of oxides is the large and ever surprising variety of properties exhibited, as well as the compositional flexibility that enables perovskites to accommodate almost every element in the periodic table.

Various structural modifications exist, some due to size incompatibilities leading to different modes of tilting of the octahedra, others such as the Brownmillerite structure, due to an ordering of oxygen vacancies. Besides these structures, which all derive from the ideal cubic perovskite, a large family of so-called hexagonal perovskites exists. Within this family, the 2H structure is the most basic one. It consists of infinite chains of face-sharing BO_6 octahedra, separated by the A cations.

Both the cubic and the hexagonal perovskite structure can be generated from the stacking of close packed $[AO_3]$ layers and the subsequent filling of the generated octahedral sites by the B cation, where an *abcabc...* type stacking results in the cubic (3C) and an *abab...* stacking results in the hexagonal (2H) perovskite structure. Variation in the stacking sequence and/or the inclusion of modified layers lead to numerous different compounds that can be considered as members of homologous series, which are known as intergrowth polytypes [2].
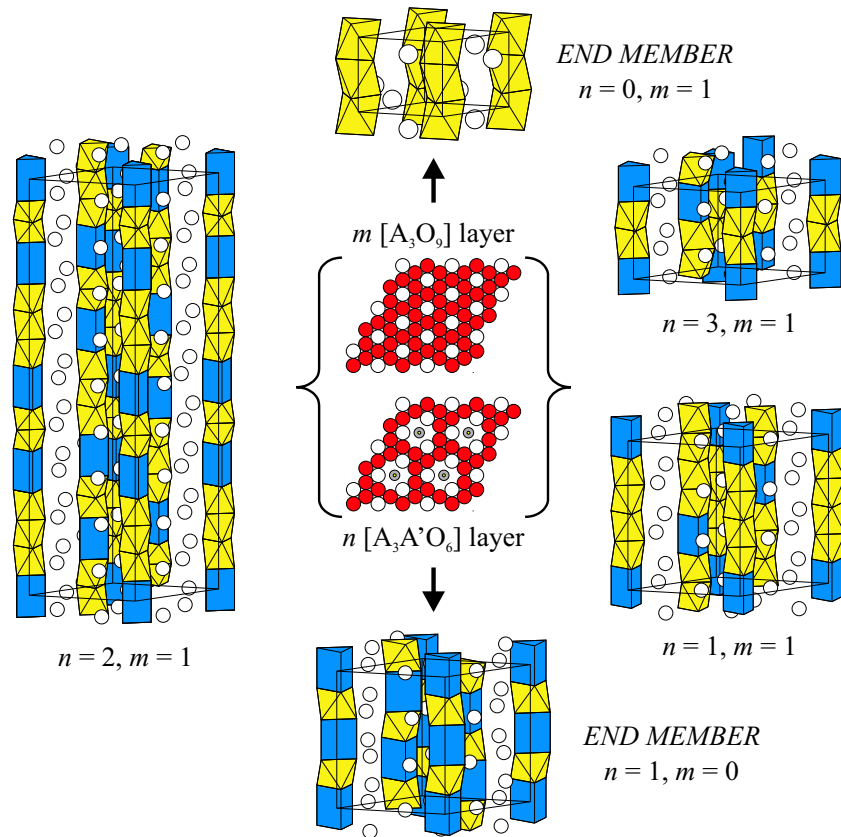
Figure 1: Scheme for the formation of the end members and some representative structures that result from the stacking of the $[A_3O_9]$ and $[A_3A'O_6]$ layers (from [3]).

For example, the incorporation of $[A_3A'O_6]$ layers leads to the $A_{3n+3m}A'_nB_{3m+n}O_{9m+6n}$ family of structures (see Fig. 1). Likewise, the incorporation of $[A_2O]$ layers leads to new structure types that are also perovskite-related. Recently, an example of such a perovskite-related structure, $Ba_5Ru_2O_{10}$, containing $[A_2O]$ layers, was reported and shown to be the $n = 3$ member of a family of phases described by the general formula $A_{n+2}B_{n-1}O_{3n+1}$ [4].

In the course of a study on the rare earth/alkaline earth ruthenate system, single crystals with the composition $La_{1.2}Sr_{2.4}RuO_7$ [5] were grown. This compound is a new A-cation deficient $n = 2$ member of the aforementioned series. Further investigations of the synthesis of polycrystalline samples [6] yielded a number of isostructural compounds belonging to the same family. Besides the structure principle of this hexagonal perovskite-intergrowth family, which may be used as a guideline for further exploiting hexagonal perovskite-intergrowth compounds, we performed systematic studies on their physical properties. The substitutions on the A and B site, respectively, lead to a slow and systematic modification of electronic and magnetic properties.

[1] R. H. Mitchell, *Perovskites: Modern and Ancient*, (Almaz Press, Thunder Bay/Ontario, 2002).

[2] J. Darriet, M. A. Subramanian, *J. Mater. Chem.* **5** (1995) 543.

[3] K. E. Stitzer, J. Darriet, H.-C. zur Loye, *Curr. Opin. Solid State Mater. Sci.* **5** (2001) 535.

[4] F. Grasset, M. Zakhour, J. Darriet, *J. Alloys Compd.* **287** (1999) 25.

[5] S. G. Ebbinghaus, *J. Solid State Chem.* **177** (2004) 817.

[6] T. Götzfried, A. Reller, S. G. Ebbinghaus, *Solid State Sci.* (2004) submitted.

2 Christian Laschinger: Magnetic Chains in Ca₃Co₂O₆

Quasi one-dimensional structures have long been acknowledged to exhibit intriguing transport and magnetic properties. New members in this family are provided by $Ca_3Co_2O_6$ [1] and a series of related iso-structural compounds A'$_3$ABO$_6$, which crystallize with the $R\bar{3}c$ structure [2]. They consist of infinite chains formed by alternating face sharing AO$_6$ trigonal prisms and BO$_6$ octahedra. Each chain is surrounded by six chains separated by Ca atoms. For $Ca_3Co_2O_6$ the Co atoms occupy both A and B sites. These Co atoms are in a 3+ configuration, but in different spin states. Cobalt atoms are strongly coupled along chains by three oxygens, while the interchain coupling is far weaker. One therefore expects that this rather unique situation gives rise to a peculiar magnetic response. As mentioned above the surrounding oxygens form two different environments in an alternating pattern. We denote the Co ion in the center of the oxygenoctahedron Co1, and the Co ion in the trigonal prisms Co2.
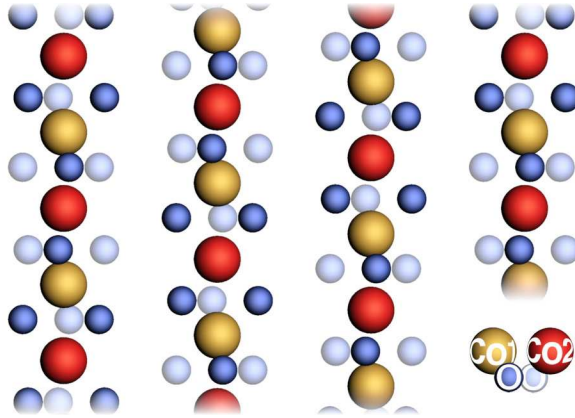
Figure 1: Projection of the Co$_2$O$_6$-chains in the (100) plane, with only those oxygen atoms drawn which are closest to the plane. Light blue spheres indicate oxygen atoms behind the plane, dark blue spheres oxygen atoms in front of the plane.

Concerning the magnetic structure, the experiments point towards a ferromagnetic ordering of the magnetic Co ions along the chains, together with antiferromagnetic correlations in the buckling a-b plane [5]. The ordering transition is reflected by a cusp-like singularity in the specific heat at 25 K [7], namely at the temperature at which one observes a strong increase of the magnetic susceptibility with lowering temperature.

The ferromagnetic order along the chains is suppressed by the frustration inherent to the lattice structure. At low temperature, this system appears to be in the partially disordered antiferromagnetic state. Moreover, several plateaus in the magnetization versus field curves are observed [1].

An appealing starting point to the understanding of the magnetic structure of a particular compound is provided by the Kanamori-Goodenough-Anderson rules [3]. Given the electronic configuration of the ions one can estimate their magnetic couplings and, at mean-field level, the magnetic ground state. In $Ca_3Co_2O_6$, the problem is more involved, in particular since each second Co^{3+} is non-magnetic, as indicated by neutron scattering data [2]. One therefore needs to determine the next-nearest neighbor magnetic coupling.

To that aim one needs i) to determine the electronic configuration of the ions, and ii) the matrix elements of the hopping operator. Both are characterized by a set of parameters obtained from an ab initio calculation, using the augmented spherical wave method [4]. The parameters which

enter the local part of the standard multi-band Hubbard Hamiltonian are the Hubbard U, the Hund's rule coupling J_H, and the crystal field splitting $10Dq$. Both U and J_H are weakly affected by the difference between the prismatic and octahedral environments.

The variation in the oxygen environment leads to three important effects. First, there is obviously a difference in the strength of the crystal field splitting, being larger in the octahedral environment. As a result Co1 is in the low spin state and Co2 in the high spin state. Second, the local energy levels are in a different sequence. For the octahedral environment we find the familiar t_{2g}–e_g splitting, provided the axes of the local reference frame point towards the surrounding oxygens. The trigonal prismatic environment accounts for a different set of energy levels. For this local symmetry one expects a level scheme with $d_{3z^2-r^2}$ as lowest level, followed by two twofold degenerate pairs d_{xy}, $d_{x^2-y^2}$ and d_{xz}, d_{yz}.

There are two, maybe competing, mechanisms for the magnetic coupling in the chains: either the coupling involves the intermediate oxygens, or direct Co-Co overlap is more important. Relying on electronic structure calculations, we may safely assume that the direct Co-Co overlap dominates [4]. The identification of the contributing orbitals is more involved. Following Slater and Koster [6] one finds that only the $3z^2$-r^2 orbitals along the chains have significant overlap. However, we still have to relate the Koster-Slater coefficients and the coefficients for the rotated frame since the natural reference frames for Co1 and Co2 differ. On the Co2 atoms with the triangular prismatic environment the z-axis is clearly defined along the chain direction, and we choose the x direction to point towards one oxygen. This defines a reference frame S. The x and y directions are arbitrary and irrelevant to our considerations. The octahedral environment surrounding the Co1 atoms defines the natural coordinate system, which we call S'. By rotating S' onto S one obtains the $3z^2$-r^2 orbital in the reference frame S as an equally weighted sum of $x'y'$, $x'z'$, $y'z'$ orbitals in S'. The above observation that the only significant overlap is due to the $3z^2$-r^2 orbitals on both Co ions now translates into an overlap of the $3z^2$-r^2 orbital on high spin cobalt with all t_{2g} orbitals on low spin cobalt.

Together these considerations lead to a local model for the interchain coupling of the magnetic Co ions. It is indeed able to explain a ferromagnetic coupling along the chain.

[1] A. Maignan, C. Michel, A. C. Masset, C. Martin and B. Raveau, Eur. Phys. J. B **15** (2000) 657.

[2] H. Fjellvåg, E. Guldbransen, S. Aasland, A. Olsen and B. Hauback, J. Sol. State Chem. **124** (1996) 190.

[3] J.B. Goodenough, Magnetism and the Chemical Bond, Wiley (New York) 1963.

[4] V. Eyert, C. Laschinger, T. Kopp and R. Frésard, Chem. Phys. Lett. **285** (2004) 249.

[5] S. Aasland and H. Fjellvåg and B. Hauback, Solid State Commun. **101** (1997) 187.

[6] J. C. Slater and G. F. Koster, Phys. Rev. **94** (1954) 1498.

[7] V. Hardy and S. Lambert, M. R. Lees and D. McK. Paul, Phys. Rev. B **68** (2003) 014424.

3   Horacio Aliaga:
Novel Algorithm for 3D Manganites

One of the most successful theoretical approachs to the study of the phase diagrams of manganites, is based on an effective model [1] that considers the competition between double-exchange (DE), superexchange (SE), and the electron-phonon interaction. The ground state of such model and the finite-temperature properties were obtained, from simulations of clusters of spins using the Monte Carlo (MC) technique together with the calculation of the electronic energies by means of exact diagonalization [2]. In order to extract useful information from the simulations, one needs to analyze different sizes for the clusters, facing an increasing computational cost. For the particular case of the standard libraries used to diagonalize the electronic matrix, the cpu memory and time scale as the number of states in the Hilbert space to the 3- and 4-power. As an example, carrying simulations on a 6x6 sites cluster, requires one week of calculation on an IBM SP4 Supercomputer and increasing the cluster size just to 8x8 would require about 2 moths. As the ED technique is actually the bottle-neck of the algorithm, it is important to by-pass it by analyzing alternative ways to obtain the electronic density of states (DOS). In this talk, I will comment on a novel technique based on the Chebyshev expansion of the time evolution operator, that allows the calculation of the electronic spectra for these type of systems. It was found that memory and cpu scales *linearly* with the number of states in the Hilbert space [3], which significantly contributes to increase the cluster size of the systems considered. A comparison with old ED results will be shown, together with the presentation of new results in 3 dimensional clusters.

[1] E. Dagotto, Nanoscale phase separation and colossal magnetoresistance, Springer-Verlag, Berlin, 2002 (and references therein).

[2] H. Aliaga, D. Magnoux, A. Moreo, D. Poilblanc, S. Yunoki, and E. Dagotto, PRB 68, 104405 (2003).

[3] V. V. Dobrovitski, M. I. Katsnelson, B. N. Harmon, Phys. Rev. Lett. 84, 3458 (2000). H. de Raedt and V. V. Dobrovitski, preprint quant-ph/0301121.

4 Robert Fichtl: Dielectric Spectroscopy and its Application to Transition-Metal Chalcogenides

In recent years, dielectric spectroscopy has proven an extremely valuable experimental method, not only in such classical applications as the investigation of the reorientational dynamics of dipolar molecules [1] but also, e.g., in the field of electronically highly correlated materials where information on the nature of charge transport and polarization effects can be gained [2]. One of the great advantages of dielectric spectroscopy is the broad dynamic range accessible, which can be achieved by the combination of different experimental techniques.

In my contribution, I will give an overview of the experimental techniques used in dielectric spectroscopy, especially the autobalance-bridge technique, the so-called frequency-response analysis, and the coaxial reflection technique, together covering a frequency range from μHz to some 10 GHz [3]. In addition, an equivalent circuit description will be introduced, which allows for the separation of intrinsic and contact effects, the latter often impeding the proper evaluation of dielectric data.

The numerous applications of dielectric spectroscopy in condensed matter physics will be briefly discussed, e.g. the investigation of the relaxational behavior of dipolar entities in glass-formers or ferroelectrics, the divergence of the dielectric constant at the metal-insulator-transition, or the hopping transport of Anderson-localized charge carriers. On two examples of recent work from our group I want to have a closer look:

Colossal Dielectric Constants

Recent reports on the observation of colossal dielectric constants (CDCs) in $CaCu_3Ti_4O_{12}$ (CCTO) reaching values up to 10^5 have generated considerable interest in this material and related compounds [4]. However, shortly after the reports of the CDCs, their intrinsic nature has been questioned and arguments have been put forth that extrinsic effects as contributions from the electrode/sample interface or from grain boundaries may be the sources of the observed CDCs [5]. To help clarifying this question, we have investigated the dielectric properties of CCTO in a broad temperature and frequency range extending up to 1.3 GHz [6]. A detailed equivalent circuit analysis of the results and two crucial experiments, employing different types of contacts (Fig. 1) and varying sample thickness, provide clear evidence that the apparently colossal values of the dielectric constant in CCTO are non-intrinsic and due to electrode polarization effects. The intrinsic properties of CCTO are characterized by charge transport via hopping of localized charge carriers and a relatively high dielectric constant of the order of 100.

Orbital Freezing

Recently, evidence for an orbital glass state in single-crystalline $FeCr_2S_4$ was deduced from specific heat measurements [7]. We have shown, that, as in $FeCr_2S_4$ the elastic response of the ionic lattice is coupled to the orbital reorientations via electron-phonon interaction, dielectric spectroscopy also reveals valuable information on the orbital freezing process [8]. Broadband dielectric spectroscopy has been performed on single-crystalline $FeCr_2S_4$ revealing a transition into a low-temperature orbital glass phase and on polycrystalline $FeCr_2S_4$ where long-range orbital order is established via a cooperative Jahn-Teller transition. The freezing of the orbital moments is revealed by a clear relaxational behavior of the dielectric permittivity (Fig. 2), which allows a unique characterization of the orbital glass transition. The mean relaxation time, the distribution of relaxation times, and the temperature dependence of the relaxation
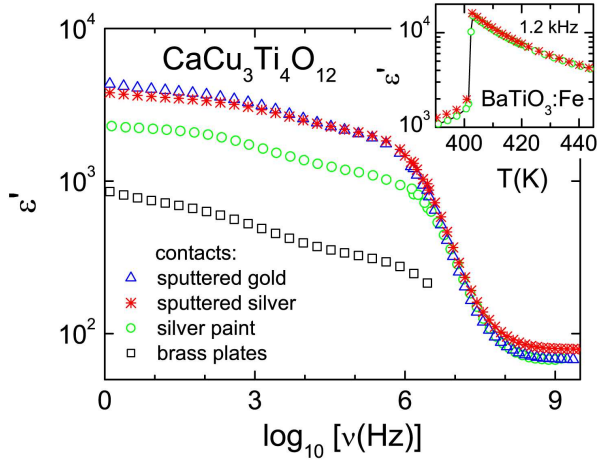
Figure 1: Frequency-dependent dielectric constant at room temperature of a CCTO sample [6], prepared with different contact types. At the lower frequencies CDCs are observed, which however strongly depend on the contact type, thus proving their non-intrinsic nature. The inset shows $\varepsilon'(T)$ of Fe-doped ferroelectric $BaTiO_3$ close to T_c, measured with silver paint and sputtered silver contacts.
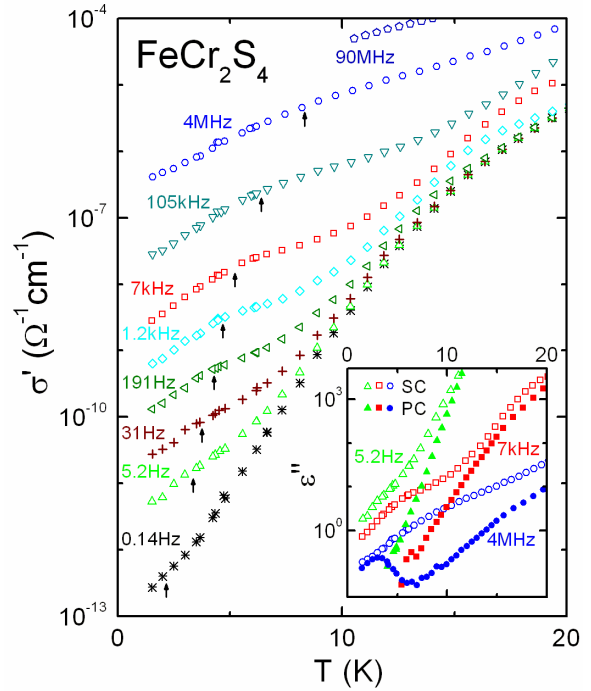
Figure 2: Temperature dependence of the conductivity in single crystalline $FeCr_2S_4$ for various frequencies [8]. The shoulders, shifting to higher temperatures with increasing frequency (arrows), reveal the typical signature of relaxational behavior, giving evidence for the glassy freezing of orbital dynamics. Inset: Comparison of the dielectric loss in single and polycrystalline material.

strength are derived. The orbital relaxation dynamics continuously slows down over six decades in time, before at the lowest temperatures the glass transition becomes suppressed by quantum tunneling. The low-temperature charge transport in $FeCr_2S_4$ is dominated by tunneling of polaronic charge carriers.

[1] see, e.g., P. Lunkenheimer *et al.*, Phys. Rev. Lett. **77**, 318 (1996); P. Lunkenheimer *et al.*, Contemp. Phys. **41**, 15 (2000).

[2] see, e.g., P. Lunkenheimer *et al.*, Phys. Rev. Lett. **69**, 498 (1992); P. Lunkenheimer and A. Loidl, Phys. Rev. Lett. **91**, 207601 (2003); P. Lunkenheimer *et al.*, Phys. Rev. B **68**, 245108 (2003).

[3] U. Schneider, P. Lunkenheimer, A. Pimenov, R. Brand, and A. Loidl, Ferroelectrics **249**, 89 (2001).

[4] C.C. Homes *et al.*, Science **293**, 673 (2001).

[5] L. He *et al.*, Phys. Rev. B **65**, 214112 (2002); D.C. Sinclair *et al.*, Appl. Phys. Lett. **80**, 2153 (2002); P. Lunkenheimer *et al.*, Phys. Rev. B **66**, 052105 (2002).

[6] P. Lunkenheimer, R. Fichtl, S.G. Ebbinghaus, and A. Loidl, cond-mat/0403119.

[7] V. Tsurkan *et al.*, preprint.

[8] R. Fichtl *et al.*, cond-mat/0404737.

5 David Schrupp: Polaronic Physics of Magnetite

Magnetite is one of the most intensively studied oxides because of its magnetic and electrical properties derived from strong electron correlations. Recently Fe_3O_4 has gained interest because of its high potential for applications in spin-electronics. In this talk the focus is on the spectral line shape of the photoemission spectra near the chemical potential and around the so called Verwey transition. This is a first-order phase transition characterized by a typical jump in resistivity of two orders of magnitude at the transition temperature ($T_V \approx 123$ K). Although now known for 65 years not only the driving mechanism but also the type of transition (metal-insulator or insulator-insulator) is still unclear.

Verwey interpreted this jump by ordering of Fe^{2+}- Fe^{3+}-ions on the B-sublattice of the inverted spinel structure of magnetite. Quite early on Anderson [2] pointed out that the short range part of the Coulomb interaction is minimized by different configurations of these ions. This findings led him to the so called Anderson condition where short range order is maintained across the transition but long range order of this configuration is lost. The driving force of the Verwey transition would then be charge ordering. However recent structure refinement on the low temperature structure by Wright et. al [1] does not corroborate this theory.

The problem of these pure Coulomb arguments is the neglect of elastic lattice energy, because strong coupling to the lattice and the formation of small polarons also play an important role in magnetite as indicated by, e.g., the small carrier mobility [2], the unusual temperature behavior of the conductivity above T_V, and the optical conductivity [3].

We studied the Verwey transition by photoemission using soft x-ray at the Fe 2p-3d absorption edge,which leads to an enhanced probing depth compared to conventional photoemission. Together with different surface preparation methods we thus are able to distinguish the bulk spectrum from surface effects. The spectra show a sharp first-order phase transition (Fig. 1)
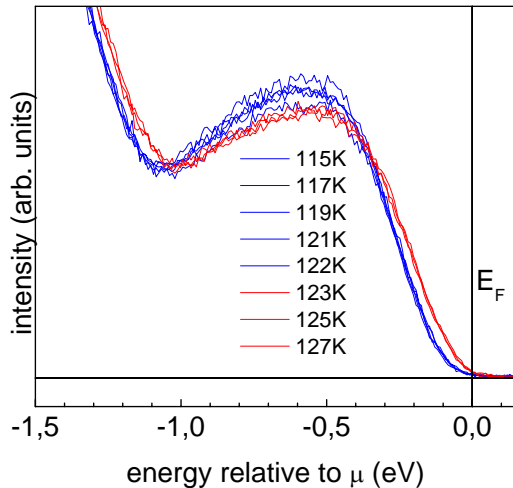
Figure 1: Spectra of a fractured sample taken around the Verwey transition temperature $T_V = 123$K near the Fermi level.
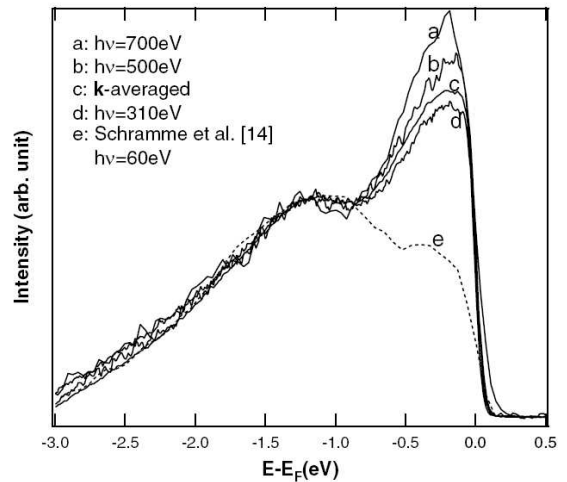
Figure 2: PES spectra of V_2O_3 taken with various $h\nu$, consistent with the Mott-Hubbard model.

but differ from that of other oxides as, e.g., V_2O_3 with Mott-like metal-insulator transitions consisting of quasiparticle (QP) peak and lower Hubbard band (Fig. 2). We analyze the bulk spectral line shape and demonstrate that it can be understood from strong electron-phonon coupling.

According to Alexandrov [4] the electron removal spectrum of such a system consists of (i) a quasiparticle (electrons heavily dressed by phonon excitations) whose spectral weight is reduced by a factor e^{-g^2} where $g^2 = \epsilon_P/\omega_0$ is a dimensionless electron-phonon coupling constant, ω_0 a characteristic phonon energy and ϵ_P the polaronic binding energy, and (ii) a series of phonon satellites shifted by multiples of ω_0 which carry the remaining weight. We used this model to account for the polaronic effects in the photoemission spectra and obtained very good fits (see Fig. 3). The value for $g^2 \approx 5$ is in good agreement with the polaronic binding energy $\epsilon_P \approx$
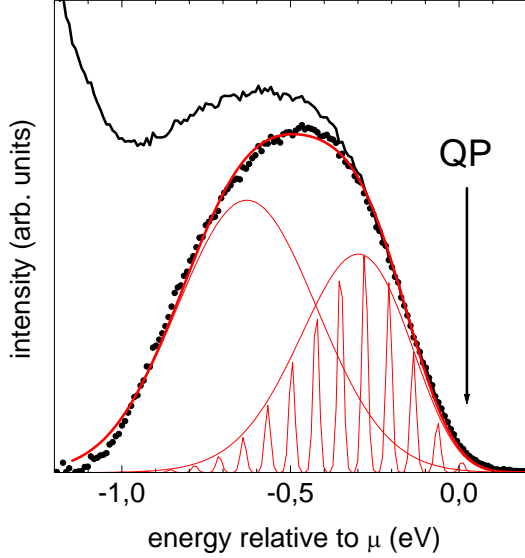
Figure 3: Theoretical fit of the background-subtracted spectrum using the polaronic single-particle spectrum of Ref. [4] with two different experimental resolutions.
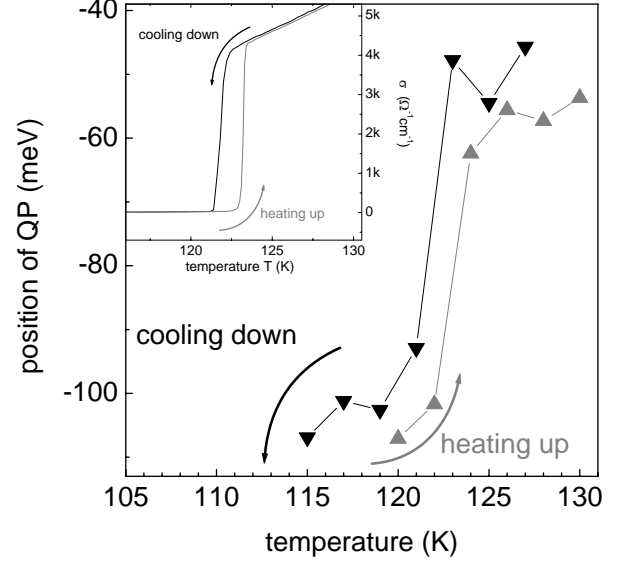
Figure 4: QP position during cooling(down-triangles) and heating (up-triangles). Also shown is the conductivity hysteresis (inset) measured on the same sample.

300meV and the effective polaron mass ($\sim 100 \ldots 200 m_0$) derived from infrared spectroscopy [3]. Furthermore, with this model we are able to determine the position of the exponentially suppressed QP band (Fig. 4). The QP position jumps exactly at T_V and is even consistent with the hysteretic behavior of the conductivity (Fig.4, inset), indicating that the spectra (Fig. 1) reflect intrinsic bulk behavior. It is found that the QP position remains *below* μ just above the Verwey temperature, which identifies the transition as of the insulator-insulator type. This conclusion is further supported by recent optical conductivity measurements by Pimenov et. al [5].

[1] J. P. Wright, J. P. Attfield, and P. G. Radaelli, Phys. Rev. Lett. **87** 266401 (2001); Phys. Rev. B **66**, 214422 (2002).

[2] N. Tsuda, K. Nasu, A. Yanase, and K. Siratori, *Electronic Conduction in Oxides* (Springer, Berlin, 1991)

[3] L. V. Gasparov *et al.*, Phys. Rev. B **62**, 7939 (2000).

[4] A. S. Alexandrov and J. Ranninger, Phys. Rev. B **45**, 13109 (1992).

[5] A. Pimenov, to be published

6 Ivan Leonov:
Charge and Orbital Order in Fe_3O_4

Magnetite (Fe_3O_4), the famous lodestone, has been known to mankind for several thousand years already. But even today, despite a long record of investigations, its low-temperature properties are still not well understood. This, together with the possible technological importance of Fe_3O_4 for spintronics, makes magnetite a material of considerable current interest. Magnetite is a mixed-valent system and is the parent compound for magnetic materials such as maghemite (Fe_2O_3) and spinel ferrites. At room temperature Fe_3O_4 is a poor metal with a moderate electronic conductivity of 4 mΩ cm. Upon further cooling its conductivity abruptly decreases by two orders of magnitude at $T_V \sim 120$ K, and the structure distorts from cubic to monoclinic symmetry. According to Verwey, who discovered this first-order metal-insulator transition, this transition is caused by charge ordering (CO) [1, 2]. He proposed a simple charge ordering model: charge arrangement of (001) planes of octahedral Fe_B atoms in the inverted spinel structure alternately occupied by 2+ and 3+ cations (the Verwey charge ordering model). This particular charge order obeys the so-called Anderson criterion for minimal electrostatic repulsion leading to a short range CO pattern, namely tetrahedra of B-sites with an equal number of 2+ and 3+ cations [3]. Many theoretical models for the low-temperature phase of magnetite have been proposed. They include purely electronic and electron-phonon models for CO, as well as a bond dimerized ground state without charge separation [4].

Recently, the low-temperature structure of magnetite was refined using high resolution x-ray and neutron powder diffraction data [5, 6]. Using the refined crystal structure we recently investigated charge and orbital ordering in magnetite by the LSDA+U method [7]. We find a charge and orbitally ordered insulator with an energy gap of 0.18 eV (Figure 1), which is in a good agreement with the experimental value of 0.14 [8]. The charge ordered ground state obtained thereby is described by a dominant [001] charge density wave with a minor $[00\frac{1}{2}]$ modulation (Figure 2). The CO coincides with the earlier proposed class-I CO [5, 6] and confirms a violation of the Anderson criterion [3]. While the screening of the charge disproportion is so effective that the total $3d$ charge disproportion is rather small (0.23), the charge order is well pronounced with an order parameter defined as a difference of $t_{2g\downarrow}$ occupancies of 2+ and 3+ Fe_B cations (0.7). This agrees well with the result of bond valence sum analysis for monoclinic structure (0.2). The orbital order is in agreement with the Kugel-Khomskii theory and corresponds to the local distortions of oxygen octahedra surrounding Fe_B-sites.

[1] E.J. Verwey, Nature (London) **144**, 327 (1939).

[2] E.J. Verwey, P.W. Haayman, and F.C. Romeijn, J. Chem. Phys. **15**, 181 (1947).

[3] P.W. Anderson, Phys. Rev. **102**, 1008 (1956).

[4] J. García, G. Subías, M.G. Proietti, H. Renevier, Y. Joly, J.L. Hodeau, J. Blasco, M.C. Sánchez, and J.F. Bérar, Phys. Rev. Lett. **85**, 578 (2000).

[5] J.P. Wright, J.P. Attfield, and P.G. Radaelli, Phys. Rev. Lett. **87**, 266401 (2001).

[6] J.P. Wright, J.P. Attfield, and P.G. Radaelli, Phys. Rev. B **66**, 214422 (2002).

[7] I. Leonov, A.N. Yaresko, V.N. Antonov, M.A. Korotin, and V.I. Anisimov, cond-mat/0402363 (2004).
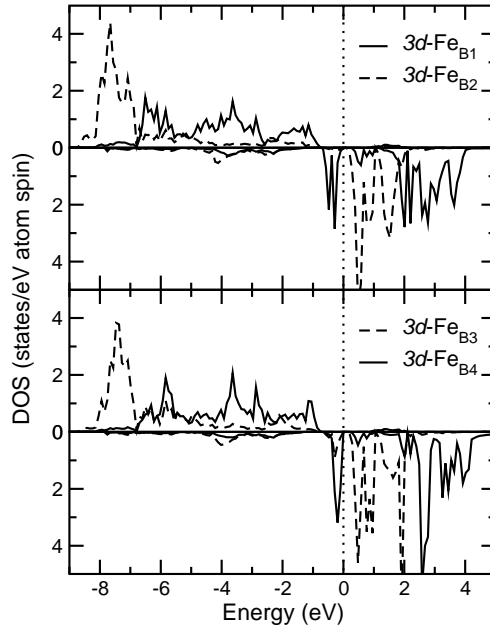
Figure 1: Partial DOS obtained from the LSDA+U calculations with U=5 eV and J=1 eV for the low-temperature $P2/c$ phase of Fe_3O_4. The top of the valence band is shown by dotted lines.
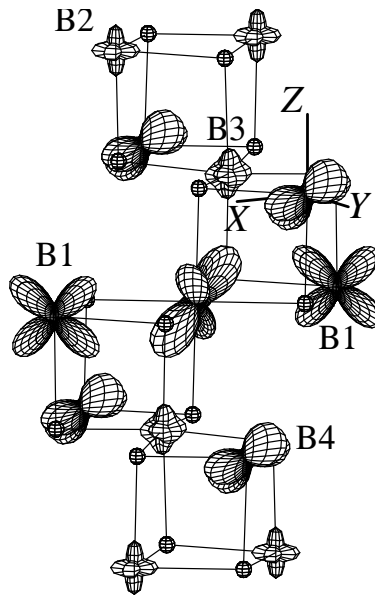
Figure 2: The LSDA+U angular distribution of the minority spin $3d$ electron density of Fe_B cations for the low-temperature $P2/c$ phase of Fe_3O_4. The angular distribution is calculated according to $\rho(\theta, \phi) = \sum_{m,m'} n_{m,m'} Y_m^*(\theta, \phi) Y_{m'}(\theta, \phi)$, where $n_{m,m'}$ is the occupation matrix of d minority states for Fe_B atoms. $Y_m(\theta, \phi)$ are the corresponding spherical harmonics. Oxygen atoms are shown by small spheres. The size of the orbital corresponds to its occupancy.

[8] S.K. Park, T. Ishikawa, and Y. Tokura, Phys. Rev. B **58**, 3717 (1998).

14

7 Daniela Schneider:
Bipolaron Formation: A comparison of the Hubbard-Holstein and the $E \otimes \beta$-Jahn-Teller-Hubbard model

We study the properties of a dilute electron gas, where electrons with two orbitals per lattice site are considered. The simplest model which includes both the local electron-lattice interaction of the Jahn-Teller type and the electronic correlations is the $E \otimes \beta$-Jahn-Teller-Hubbard model. In particular we consider the symmetry-breaking β_1-mode. This symmetry-breaking vibrational mode can couple linearly to the difference of the electronic orbital densities. We analyze the formation and stability of Jahn-Teller polarons and bipolarons, respectively. Our approach is based on a hopping expansion in the strong-coupling regime. The results are compared with findings for the Holstein-Hubbard model [1, 2], in which the electronic density is coupled to symmetry-conserving ligand deformations. After a convenient Lang-Firsov transformation the $E \otimes \beta$-Jahn-Teller-Hubbard Hamiltonian is given as follows

$$
\begin{aligned}
H &= H_{\text{t}} + H_0 \\
H_{\text{t}} &= -t \sum_{\langle ij \rangle \gamma \sigma} \left(c_{i\gamma\sigma}^+ c_{j\gamma\sigma} \, X_{i\gamma}^+ X_{j\gamma} \; + \; \text{H.c.} \right) \\
H_0 &= \sum_{i\gamma} \left((U - 2E_{\text{p}}) \, n_{i\gamma\uparrow} n_{i\gamma\downarrow} \; + \; \frac{1}{2} \left(U_{\theta\epsilon} + 2E_{\text{p}} \right) n_{i\gamma} n_{i\bar{\gamma}} \right) \\
&\quad + \hbar\omega \sum_i b_i^+ b_i \; - \; E_{\text{p}} \sum_{i\gamma} n_{i\gamma} \qquad \text{with} \quad \bar{\gamma} = -\gamma = \theta, \epsilon \;\;, \;\; n_{i\gamma} = n_{i\gamma\uparrow} + n_{i\gamma\downarrow} \;.
\end{aligned}
\tag{1}
$$

$X_{i\theta}^+ = X_{i\epsilon} = e^{-g(b_i^+ - b_i)}$ are the shift-operators and $E_{\text{p}} = g^2 \hbar\omega$ is the energy gain with the electron-phonon coupling constant g. Two electrons on a lattice are considered. In the regime of attractive on-site interaction ($U < 2E_{\text{p}}$) one finds the degenerate ground state of H_0 as an on-site bipolaron $c_{i\gamma\uparrow}^+ c_{i\gamma\downarrow}^+ |0\rangle$ (S0). We restrict ourselves to the case of repulsive on-site interaction ($U > 2E_{\text{p}}$). If both electrons are in the same orbital, the situation is exactly that of the Holstein-Hubbard model [1, 2]. For a square lattice the hopping expansion leads to an exponentially reduced hopping te^{-g^2} in first order. The second order hopping processes

Figure 1: Hopping processes in second order for electrons in the same orbital. The lowered lines represent sites with energy shift E_{p} and $2E_{\text{p}}$, respectively. The spatial shift is not shown.

Figure 2: Hopping processes in second order, that do not change n_i for electrons in different orbitals. The spatial and energy shift is not shown.

are shown in Fig. 1. On the right hand site the correction in energy of the corresponding process is given in strong coupling approximation. The exact formulas are infinite sums in powers of g^2 and $2g^2$, respectively. Notice that if there is no change in the lattice configuration, the exponential prefactor cancels and therefore we consider only these terms. In the basis $c^+_{i\gamma\downarrow}c^+_{i+a\gamma\uparrow}|0\rangle$, $c^+_{i+a\gamma\downarrow}c^+_{i\gamma\uparrow}|0\rangle$ ($a > 0$) the matrix is diagonal for all $a > 1$ and due to e) there is a 2×2 block for $a = 1$. One has to take the coordination number of the lattice into account and finds for the square lattice in this approach a dimensional-independent binding energy $\Delta = \frac{t^2}{E_p} - \frac{4t^2}{U}$ for the $a = 1-$spin singlet state (S1). This is the ground state if $2E_p < U < 4E_p$. Furthermore there is a triplet state and $a > 1-$states between these levels. The other configuration corresponds to electrons in different orbitals. One finds that the electron exchange for different levels b2) in Fig. 2 – comparable with the process e2) in Fig. 1 – is also exponentially reduced, actually with a prefactor e^{-4g^2}. The reason is the change of the spatial distortion at both lattice sites. Therefore the second order hopping matrix, neglecting the exponentially reduced terms, is diagonal for states with different orbitals. The energy for $a = 1-$states of different orbitals lies between the $a > 1-$states and the triplet states for the single orbital. The ground state remains the S1-bipolaron.
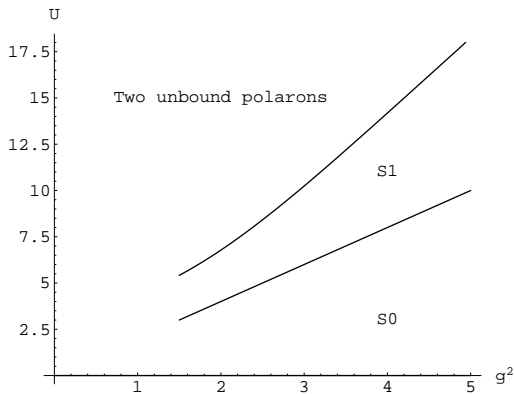
Figure 3: Phase diagram for two electrons in the same orbital, valid in the strong coupling regime. S0 and S1 labels the on-site- and nearest-neighbor-bipolaron, respectively. The phase boundary S0-S1 is given by $U = 2E_p$. The S1-phase is separated from the free polarons by $\Delta = 0$.

[1] A. Macridin, G. A. Sawatzky and Mark Jarrell, *cond-mat*/0401305.

[2] J. Bonča, T. Katrašnik and S. A. Trugman, *Phys. Rev. Lett.* **84**, 3153 (2000).

8 Carmen Mocanu: Finite Size Bosonization and Self-Consistent Harmonic Approximation

Bosonization techniques have been extensively used in the study of one-dimensional electron and spin systems [1, 2, 3]. The success of the method is based on the fact that the low energy properties of fermions are determined by the states close to the Fermi surface, which in one dimension consists only of two points. When the spectrum is linearized around the Fermi points the Hamiltonian can be expressed in terms of free bosons associated with particle-hole excitations of momentum q.

Perturbations like impurity scattering or a modulation of the hopping lead to nonlinearities in the bosonized Hamiltonian and require to introduce extra operators, the so-called Klein factors. Since an exact solution is known only in some special cases [4], one has, in general, to resort to approximative methods like renormalization group calculations. Another more intuitive method is the self-consistent harmonic approximation (SCHA), originally introduced for the sine-Gordon model [5], where the non-linear terms are replaced by a harmonic potential with parameters to be determined self-consistently according to a variational principle for the energy. Since the SCHA is a non-perturbative method it is well-suited for situations where the non-linear terms drive the system into a different phase.

The SCHA has been successfully applied to various non-linear field theories [5, 6, 7]. In the context of bosonized Hamiltonians, however, the existence of Klein factors has been ignored in these approaches. Here, we present an extension of the SCHA which treats the bosonic fields and the Klein factors on equal footing [8]. As a prototype model for this study we consider the lattice model of spinless fermions at half filling including nearest-neighbor interaction and a modulation of the hopping due to a periodic lattice distortion, described by the following Hamiltonian

$$
\begin{aligned}
H \;=\; & -t\sum_i (1 + (-1)^i u)(c_i^+ c_{i+1} + c_{i+1}^+ c_i) \\
& + V\sum_i n_i n_{i+1}
\end{aligned}
\tag{1}
$$

where u is the dimerization parameter that leads to a periodic modulation of the hopping amplitude t, and V is the strength of the nearest-neighbor interaction. At half filling and in the range $-2 < V/t < 2$ the bosonized Hamiltonian of this model reads [2]

$$
\begin{aligned}
H \;=\; & \int_0^L \frac{\mathrm{d}x}{2\pi}\left\{ \frac{v}{g}\,{:}(\partial_x \phi)^2{:} + vg\,{:}(\partial_x \theta)^2{:} \right\} + \frac{\pi v}{2Lg}N^2 \\
& + \frac{\pi v g}{2L}J^2 - \frac{itu}{\pi a}\int_0^L \mathrm{d}x\; F_L^+ F_R\, \mathrm{e}^{2i\phi(x)} + h.c.
\end{aligned}
\tag{2}
$$

where ϕ and θ are conjugate fields, and a is cut-off parameter of the order of the lattice spacing. The renormalized Fermi velocity $v = \pi t \sin(2\eta)/(\pi - 2\eta)$ and the Luttinger parameter $g = \pi/4\eta$ are related to the interaction according to $V = -2t\cos(2\eta)$. The normal ordering operation $({:}\;\;{:})$ is introduced to avoid the divergences associated with unphysical states assumed by the Luttinger model. N and J are the charge and current operators, defined as $N = N_L + N_R$ and $J = N_L - N_R$, respectively, where N_L and N_R count the number of left and right moving particles with respect to the filled Fermi sea. The Klein factors $F_{L/R}^+$ and $F_{L/R}$ rise or lower the number of left and right moving fermions by one (which no combination of bosonic operators can ever do), and they assure also that fermions of the two different species anticommute. The

dimerization, described by the non-linear term of the Hamiltonian, breaks the conservation of the current J and is responsible for the opening of an energy gap. To discuss the gap formation quantitatively, we construct an exactly solvable trial Hamiltonian H_{tr} where the bosonic fields in (2) are decoupled from the Klein factors and where the non-linear terms $\sim \mathrm{e}^{\pm 2i\phi}$ are replaced with a quadratic form $\sim \phi^2$. Accordingly we choose $H_{\mathrm{tr}} = H_{\mathrm{tr}}^{\Delta} + H_{\mathrm{tr}}^{B}$ as the sum of two commuting parts

$$H_{\mathrm{tr}}^{\Delta} = \int_0^L \frac{\mathrm{d}x}{2\pi} \left\{ \frac{v}{g}(\partial_x \phi)^2 + vg(\partial_x \theta)^2 + \frac{\Delta^2}{vg}\phi^2(x) \right\} \tag{3}$$

and

$$H_{\mathrm{tr}}^{B} = -iB(F_L^+ F_R - F_R^+ F_L) + \frac{\pi vg}{2L}J^2 \tag{4}$$

each of them depending on a single variational parameter, Δ and B, respectively. Notice that from the standard trial Hamiltonian alone (Eq. (3)), only the trivial solution $\Delta = 0$ can be obtained. Therefore the non-standard term Eq. (4) is necessarily required to describe the phase transition in the system.

Concerning the energy, we find the following results. For the infinite system, both the value of the Luttinger parameter $g = 2$ ($V/t = -\sqrt{2}$) where the transition from a gapless to a gapped phase takes places and the exponent $1/(2 - g)$ that characterizes the opening of the gap for $u \to 0$ are correctly obtained within the SCHA. However, the bending of the phase boundary for finite values of u is not reproduced. When considering a finite system Klein factors cannot be ignored. Within our approach it turns out, that the crossover region from a finite size gap to a true dimerization gap coincides with the crossover to the region where the Klein factors become relevant.

As a second application of the method, we calculate the Drude weight, which reflects the sensitivity of the system with respect to a change of boundary conditions and is related to the properties of the current operator J in the bosonized version of the Hamiltonian. In a finite system with an energy gap Δ the Drude weight is expected to be nonzero but exponentially small, $D \sim \exp(-\mathrm{const} \cdot L\Delta)$. Our extended version of the SCHA allows to calculate the Drude weight in the insulating phase and we confirm the exponential behavior.

[1] F. D. M. Haldane *Phys. Rev. Lett.* **47** 1840 (1981)

[2] J. von Delft and H. Schoeller *Ann. Phys. (Leipzig)* **7** 225 (1998)

[3] H. J. Schulz, G. Cuniberti and P. Pieri *Field Theories for Low-Dimensional Condensed Matter Systems: Spin Systems and Strongly Correlated Electrons* ed G. Morandi *et al* (New York: Springer) (2000)

[4] R. J. Baxter *Exactly Solved Models in Statistical Mechanics* (New York: Academic Press (1982)

[5] S. Coleman *Phys. Rev. D* **11** 2088 (1975)

[6] H. Fukuyama and H. Takayama *Electronic Properties of Inorganic Quasi-One-Dimensional Compounds* ed P. Monceau (Dordrecht: D. Reidel) (1985)

[7] C. Schuster and U. Eckern *Eur. Phys. J. B* **5** 395 (1998)

[8] C. Mocanu, M. Dzierzawa, P. Schwab and U. Eckern submitted to *J. Phys.: Condens. Matter*

9 Georg Eickerling, Dmitry Shorokhov, Wolfgang Scherer: Occurrence and Consequences of Charge Concentrations in Transition Metal Oxides

During the past few years analysis of the topology of the charge density has emerged as one of the leading experimental tools to investigate the electronic structures of a wide range of compounds, including molecular complexes and solid state compounds.[1]

Recent charge density studies[2, 3] show that formation of local charge concentrations (CCs) in the valence shell of transition metal atoms might dominate and control the coordination geometry of transition metal compounds and also influence their chemical and physical properties.[4] The impact of CCs on the geometry of transition metal oxides in the solid state has been investigated by a study on the polymeric compound of methyltrioxorhenium (MTO), $\{(CH_3)_{0.9}ReO_3\}_\infty$. This compound, in the following denoted *poly*-MTO, consists of a two-dimensional $[ReO_2]_\infty$ network. In the third dimension the Rhenium coordination is completed by an oxo-group on one side and a methyl-group on the other side of the $[ReO_2]_\infty$ layers. When the structure-determining rôle of these CCs is taken into account a non-octahedral geometry of the $[ReO_5C]$ framework should result. Indeed, quantum-chemical calculations at the B3LYP/LANL2DZ level predict pronounced ligand-opposed charge concentrations in the valence shell of the rhenium atoms of *poly*-MTO induced by covalent Re-C bonding. As a result, geometry optimizations on an extended cluster model of *poly*-MTO (see Figure 1a) at the same level of theory lead to a highly distorted equilibrium structure as depicted in Figure 1, left.

Specific heat measurements on *poly*-MTO show strongly enhanced c/T values below 3 K.[5] This is an indication for strong electron correlation effects. In addition, the resistance shows an exponential dependency of the temperature below 20 K, which is characteristic for a semiconductor while at room temperature *poly*-MTO shows a metallic behavior.[5] We suggest that this semiconductor behavior might be related to the enhancement of the *same* local CCs in the valence shell of the Rhenium atoms which were found responsible for the structural distortion of the $[ReO_5C]$ polyhedra.
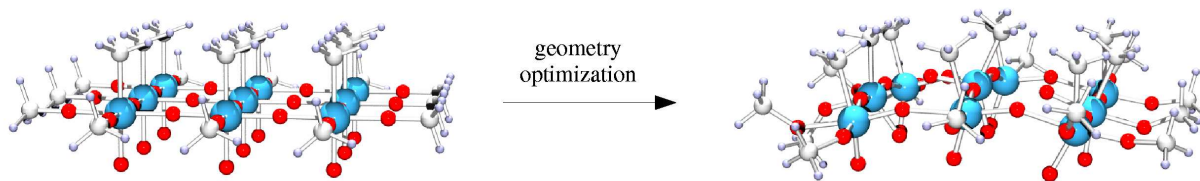
Figure 1: Geometry optimizations (B3LYP/LANL2DZ) on a molecular model of *poly*-MTO.

In a second example, the classical oxide Ti_2O_3, we demonstrate that significant CCs might not only cause semiconductor behavior in organometallic compounds at low temperatures but also control metal to insulator (MI) transitions in classical transition metal oxides.

Ti_2O_3 is known to undergo a MI transition in the broad temperature range from 350 K to 600 K. This transition is accompanied by a change in the lattice constant, c, leading to rather short Ti'···Ti" contacts of about 2.578 Å at 295 K (see Figure 2, right). Analysis of the CCs formed in the valence shell of the Ti atoms at various geometries at different temperatures employing theoretical studies at the B3LYP/8-6411G* level reveals a significant change in magnitude from about 290 eÅ^{-5} at 300 K to about 265 eÅ^{-5} at 800 K (see Figure 2). Hence, the MI transition in Ti_2O_3 appears reflected in a dramatic increase of the bonding charge concentrations (BCCs)

in the valence shell of the paired titanium atoms Ti' and Ti" (see Figure 2). Hence, formation of localized CCs at the Ti atoms reduces the charge density of the itinerant electrons in Ti_2O_3 at temperatures below $800\,\mathrm{K}$ which might be the origin of the MI transition in this extensively studied compound.
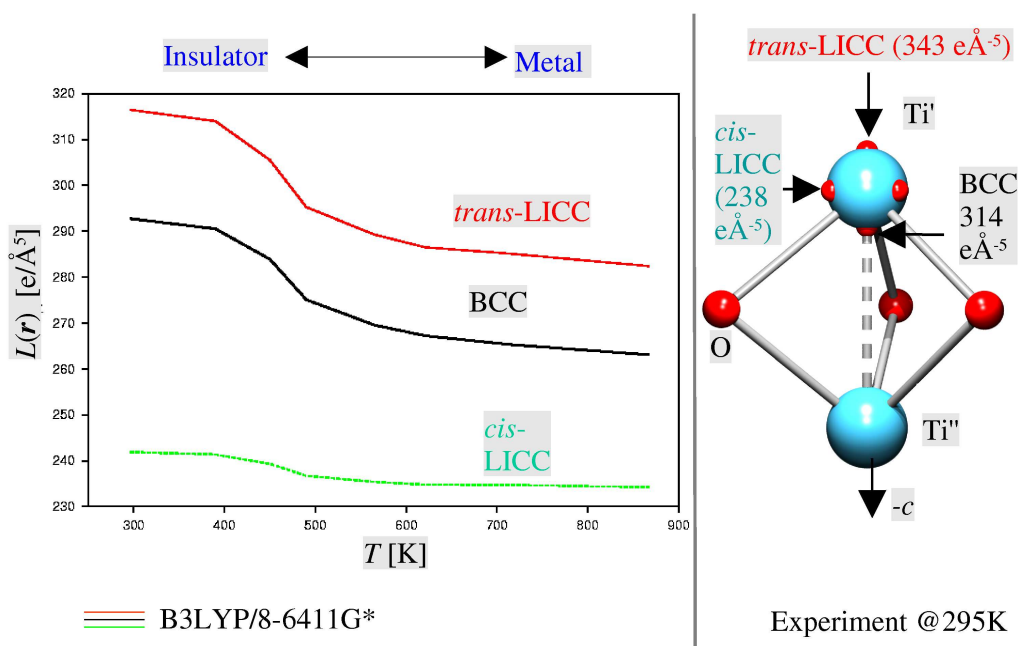
Figure 2: Left: Temperature dependence of all three types of charge concentration in the valence shell of Ti' obtained by calculation at the B3LYP/8-6411G* level of theory. Right: Location and magnitude of the CCs based on high resolution X-ray diffraction experiments at $295\,\mathrm{K}$.

A new experimental charge density analysis on Ti_2O_3 based on data collected earlier [6] at $295\,\mathrm{K}$ is in good agreement with the values predicted by theory (see Figure 2). In addition, direct analysis of the multipole model allows to decide which orbitals are involved in the formation of the BCC at Ti. It can be shown, that a d_{z^2}-type orbital at the Ti atom is mainly responsible for the formation of all three types of CCs found in the valence shell of Ti: (*i*) the BCC, (*ii*) the ligand opposed charge concentration (*trans*-LICC) as well as (*iii*) the diffuse belt around the Ti atom (*cis*-LICC). This interpretation is further supported by a theoretical study on various molecular model systems of hexa-coordinated transition metal complexes using the Natural Bonding Orbital (NBO) method.[7]

[1] See, for example: T. S. Koritsanszky, P. Coppens, *Chem. Rev* **2001**, *101*, 1583-1627.

[2] W. Scherer, G. S. McGrady, *Angew. Chem. Int. Ed.* **2004**, *43*, 1782-1806.

[3] W. Scherer, G. S. McGrady et al. *Chem. Eur. J.* **2003**, *9*, 6057-6070.

[4] See, for example: R. J. Gillespie, I. Hargatti, *The VSEPR Model of Molecular Geometry*, Allyn and Bacon, Boston, 1991.

[5] R. Miller, C. Helbig et al. *Conference Proceedings for SCES* **2004**.

[6] M. G. Vincent, J. Ashkenazi, *Acta Cryst. Sec. A* **1980**, *36(SEP)*, 803-808;

[7] A. E. Reed, R. B. Weinstock, F. Weinhold, *J.Chem.Phys* **1985**, *83*, 735.

10 Verena Körting: Interface-Mediated Pairing in Field Effect Devices

In 1964 W. A. Little proposed a possible pairing mechanism for electrons in long organic molecules involving localized electronic excitations in the molecules' side chains [1]. Later, Ginzburg [2] and Allender, Bray and Bardeen [3] proposed an excitonic 2D mechanism in superconductor-semiconductor sandwiches.

We propose, that a similar scheme works for an insulating layer L2 with polarizable localized excitations in proximity with a superconducting layer L1 of near-atomic thickness [4]. Assuming that a sufficient carrier density can be induced by applying an electric field as shown in Fig. 1, we argue that superconductivity may be observable in such systems. The critical temperature is calculated as a function of applied voltage and for different materials properties.
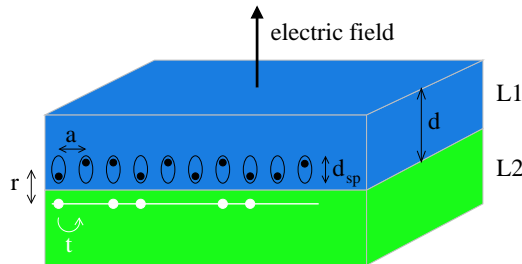
Figure 1: Proposed experimental geometry for a field effect device. Only interface between layers L1 and L2 shown.

Qualitatively, we expect the following mechanism to apply: virtual excitations in the dielectric L1 induce Cooper pairing in the adjacent layer L2. The critical temperature must increase initially with the field since carriers are being injected into the system. With increasing electric field two effects result in a decrease of the pair potential. First the larger level splitting of the two level system leads to a suppression of the polarization fluctuations and second the repulsion between a field-induced dipole in L1 and an electron in L2 increases.

We propose a crude, but concrete framework within which one can calculate these effects. The Hamiltonian of the dipole layer L1 is expressed in terms of pseudo-spin operators and treated within "linear spin wave theory". With a modified variational Lang-Firsov transformation we can identify the pairing mechanism. The variational parameters are fixed through Feynman's variational principle, which also decouples the interaction terms. Finally, the critical temperature is calculated in BCS theory.

In Ref. [4] the dependence on the critical temperature T_c for various materials properties is discussed. In Fig. 2 the dependence on electric field energy, which is proportional to the applied voltage, is shown for a dielectric constant of 100 and for an intermediate interaction. The interaction in this scheme is the Coulomb interaction between the charge carriers in the metallic layer and the dipoles in layer L1. The three data sets in Fig. 2 correspond to different level splittings $\Delta_{sp}/4t$ of the dipoles in layer L1. This energy difference is of the order of the charge transfer gap in transition metal oxides. In these compounds half the band width $4t$ is of the order of 0.4 eV.

For small increasing electric field the transition temperature is raised due to the accumulation of charge in the metallic layer (cf. Fig. 2). The electric field strength is directly related to the band filling or induced areal charge density. Strong electric fields with sizable band filling lower the transition temperature as the effective level splitting is enlarged. In fact, as seen from the $\Delta_{sp}/4t = 1.25$ curve in Fig. 2 there are two scales for the suppression of T_c at higher fields. The
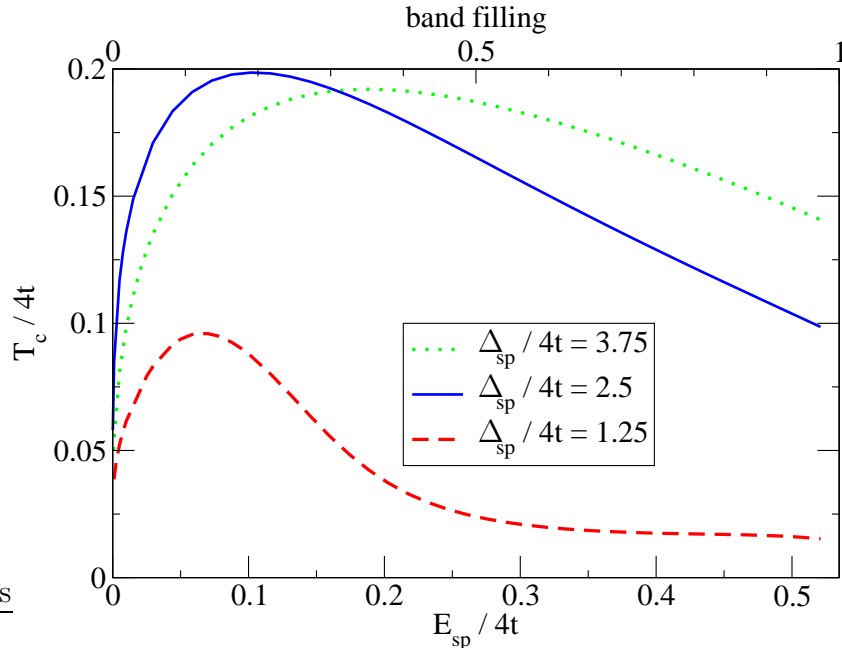
Figure 2: transistion temperature $T_c/4t$ vs. electric field energy $E_{sp}/4t$ and band filling n, lower and upper axis, respectively.

lower scale is set by repulsive terms in the effective interaction energy and is also responsible for the observed decay of T_c in the two further curves (with $\Delta_{sp}/4t = 2.5$ and 3.75). In this regime, T_c is being suppressed primarily by the increasing repulsion between the polarized dipoles and the 2D electrons, which scales with the applied field. The larger scale, which is responsible for the slow decay at even higher fields, is set by $\Delta_{sp}/4t$, and corresponds to the eventual saturation of the dipole moment.

In Fig. 2 the maximal T_c is reached for a level splitting of $\Delta_{sp}/4t = 2.5$. It has been shown [4], that

$$\Delta_{sp}/4t \approx 2.5$$

is the optimal value to observe a strong enhancement of T_c with the mechanism of interface-mediated pairing in a field effect device.

Hence, the properties of a drain source channel (DS-channel) embedded in an oxide field effect transistor will be controlled not only by the electronic and structural properties of the DS-channel, as is usually assumed, but can furthermore be strongly influenced by the gate insulator or by other adjacent dielectric layers.

In this model several potentially important aspects of the physics are not present including Coulomb interactions, dynamics of the dielectric screening and correlations in the metallic layer. We expect, however, that the qualitative dependence of T_c on the electric field will not change significantly.

[1] W.A. Little, Physical Review A **134**, 1416 (1964).

[2] V.L. Ginzburg, Physics Letters **13**, 101 (1964).

[3] D. Allender, J. Bray, and J. Bardeen, Physical Review B **7**, 1020 (1973).

[4] V. Körting, Qingshan Yuan, P.J. Hirschfeld, T. Kopp and J. Mannhart, *Interface-mediated pairing in field effect devices*, (cond-mat/0402624).

11 Alexander Weber:
The Grain Boundary Problem and its Possible Solution for Applications in High-T_c Superconductors

After the blackouts in North America and Europe in 2003, the need to modernize the power grids is obvious. A possible solution is the installation of high-T_c superconducting cables. For this, the »grain boundary problem«, which is the exponential decrease of the grain boundary critical current density J_c of the high-T_c cuprates as a function of the boundary angle [1], has to be solved.

Today, the most promising approaches to the fabrication of competitive cables from high-T_c materials operating at 77 K are the »coated conductor technologies«. These techniques aim at avoiding the deleterious effects of large angle grain boundaries on the critical current density by aligning the grains to a few degrees along all major crystal axes. Large efforts have been undertaken to develop practical methods for the fabrication of polycrystalline high-T_c superconductors with well aligned grains, of which the »ion-beam assisted deposition« (IBAD) [2, 3], the »rolling assisted biaxially textured substrate« (RABiTS) [4], and the »inclined substrate deposition« (ISD) [5, 6] processes are the most advanced. By using these techniques J_c values well above 10^6 A/cm^2 have been achieved for conductors up to several meters in length. The required precise alignment of the grains, however, is still a costly and time consuming procedure.

We have shown recently that the critical current density of grain boundaries at 4.2 K can be substantially increased by appropriate doping, for example by partially substituting Y^{3+} by Ca^{2+} in $YBa_2Cu_3O_{7-\delta}$ [7]. The increase of J_c is maintained at temperatures up to T_c if the doping at the grain boundary is performed locally by employing doping heterostructures [8].

These experiments suggest to use heterostructures also to improve coated conductors. To explore whether this is possible, we measured the effects of doping the grain boundaries on the critical current density of $YBa_2Cu_3O_{7-\delta}$ based IBAD-samples [9]. The critical current density of the investigated IBAD-tapes is enhanced by factors as large as 2.2 at all temperatures up to T_c.

Of high interest for applications is the dependence of the critical current density on an applied magnetic field. The enhancement of the critical current density of doping heterostructures on IBAD-tapes is found to persist at 77 K in fields up to 8 T and even increases in fields exceeding 6 T.

Today, the main field of application for superconducting materials are high field magnets, which are almost all made from low-T_c superconductors. It exists nevertheless a interest to further improve the achievable magnetic fields (e.g. for high field NMR). This could be reached by benefiting from the high critical fields of high-T_c superconductors. A $Bi_2Sr_2CaCu_2O_8$-tape wound into an insert magnet achieved 5 T in a background field of 20 T and thus holds the world record of reached magnetic fields with superconducting magnets at present. Unlike the application of high-T_c cables for the transport of electric current in power grids, the working temperature of such magnets is in most cases below 20 K.

We show that doping $YBa_2Cu_3O_{7-\delta}$ with Ca increases the critical current density of grain boundaries at 4.2 K and improves its magnetic field properties. $Y_{1-x}Ca_xBa_2Cu_3O_{7-\delta}$ ($x \leq 0.3$) shows great promise for coated conductor tapes wound into high field magnets to operate at low temperatures ($T \leq 20$ K).

[1] D. Dimos, P. Chaudhari, J. Mannhart and F.K. LeGoues, Phys. Rev. Lett. **61**, 219 (1988).

[2] Y. Iijima, N. Tanabe, O. Kohno and Y. Ikeno, Appl. Phys. Lett. **60**, 769 (1992).

[3] X.D. Wu, S.R. Foltyn, P.N. Arendt, J. Townsend, C. Adams, I.H. Campbell, P. Tiwari, Y. Coulter and D.E. Peterson, Appl. Phys. Lett. **65**, 1961 (1994).

[4] D.P. Norton, A. Goyal, J.D. Budai, D.K. Christen, D.M. Kroeger, E.D. Specht, Q. He, B. Saffian, M. Paranthaman, C.E. Klabunde, D.F. Lee, B.C. Sales and F.A. List, Science **274**, 755 (1996).

[5] K. Hasegawa, N. Yoshida, K. Fujino, H. Mukai, K. Hayashi, K. Sato, T. Ohkuma, S. Honjyo, H. Ishii and T. Hara, *In-plane aligned YBCO thin film tape fabricated by pulsed laser deposition, Proceedings of the International Cryogenic Engineering Conference (ICEC16), Kitakyushu, Japan (1996),* p. 1413.

[6] M. Bauer, R. Semerad and H. Kinder, IEEE Trans. Appl. Supercond. **9**, 1502 (1999).

[7] A. Schmehl, B. Goetz, R.R. Schulz, C.W. Schneider, H. Bielefeldt, H. Hilgenkamp and J. Mannhart, Europhys. Lett. **47**, 110 (1999).

[8] G. Hammerl, A. Schmehl, R.R. Schulz, B. Goetz, H. Bielefeldt, C.W. Schneider, H. Hilgenkamp and J. Mannhart, Nature **407**, 162 (2000).

[9] A. Weber, G. Hammerl, A. Schmehl, C.W. Schneider, B. Schey, M. Kuhn, R. Nies, B. Utz, H.-W. Neumueller and J. Mannhart, Appl. Phys. Lett. **82**, 772, (2003).

12 Hyun Jung Lee: Quantum Phase Transitions in Models of Magnetic Impurities

In recent years, quantum phase transitions have attracted the interest of both theorists and experimentalists in condensed matter physics [1]. These transitions, which are accessed at zero temperature by variation of a non-thermal control parameter, can influence the behavior of electronic/bosonic systems over a wide range of the phase diagram. We review our recent work on quantum phase transitions in impurity models describing the interaction of a magnetic impurity with a fermionic or a bosonic host. The common feature of both systems is a competition between two different fixed points representing the zero and the infinite coupling phase. This competition generates new unstable fixed points associated with the phase transitions.

(a)

(b)
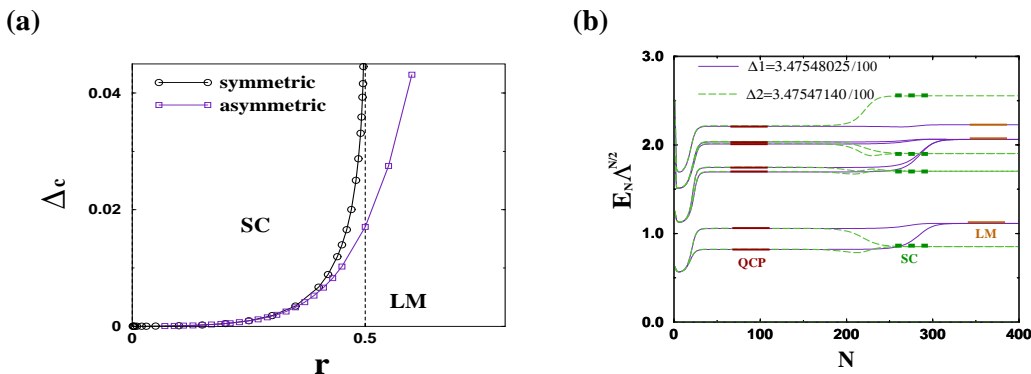
Figure 1: (a) T=0 phase diagram for the soft-gap Anderson model in the particle-hole symmetric and asymmetric case; the parameter Δ measures the hybridization strength, $\Delta(\varepsilon) \equiv \pi V^2 \rho(\varepsilon) = \Delta |\varepsilon|^r$. (b) NRG flow diagrams for $r = 0.35$, close to the phase transition

In the soft-gap Anderson model [2], the conduction band has a power-law density of state ($\rho \propto |\varepsilon|^r$) which leads to a continuous transition between a local-moment (LM) and a strong-coupling (SC) phase [3, 4]. The structure of the LM and SC fixed points can be easily understood as that of a free conduction electron chain [5]. In contrast, the structure of the quantum critical point is unclear, probably because the quantum critical point is not built up of non-interacting single-particle states.

In the spin-boson model [6], the impurity-spin couples to a bosonic bath with the coupling specified by the power-law spectral function $J(\omega) \propto |\omega|^s$. NRG calculation found that there is a line of critical points for $0 < s < 1$, which divide the phase space into the localized (L) and the delocalized (D) phase [7]. The structure of the fixed points L and D can be understood from the single particle excitations of a non-interacting bosonic system but the quantum critical points cleary show non-trivial behaviour.

The impurity contribution to the entropy (S_{imp}) was also calculated for various α. The residual entropy changes from $\ln 2$ to zero as the systems goes from the localized to the delocalized phase. At the quantum critical point α_c, the entropy, extracted from the unstable fixed points, takes a value between zero and $\ln 2$ depending on the bath exponent s.

[1] R. Bulla and M. Vojta, cond-mat/0210015 (2002)

[2] D. Withoff and E. Fradkin, Phys. Rev. Lett. **64**, 1835 (1990)

[3] R. Bulla, T. Pruschke and A. C. Hewson, J. Phys.: Condens. Matter **9**, 10463 (1997)
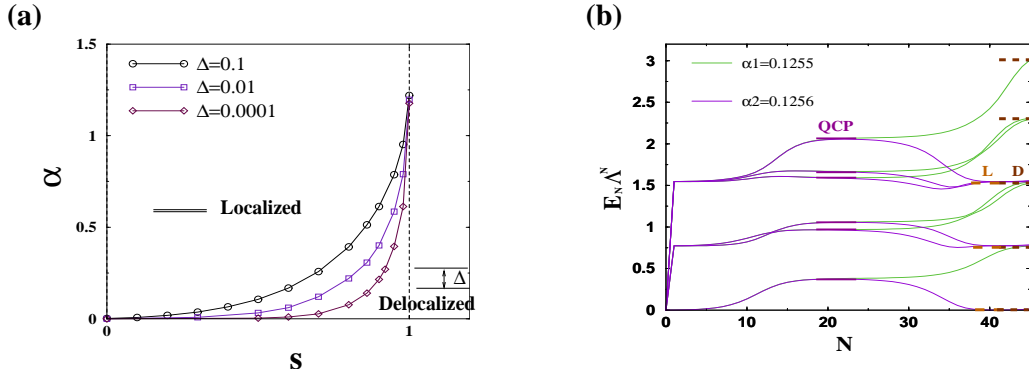
Figure 2: (a) Phase diagram for the transition between the delocalized ($\alpha < \alpha_c$) and the localized phase ($\alpha > \alpha_c$) of the spin-boson model for various values of Δ. The dimensionless parameter α characterizes the dissipation strength. (b) NRG flow diagrams for $s = 0.8$, close to the phase transition.

[4] C. Gonzalez-Buxton and K. Ingersent, Phys. Rev. B **57**, 14254 (1998)

[5] K. G. Wilson, Rev. Mod. Phys., **47** (1975)

[6] A. J. Leggett et al., Rev. Mod. Phys., **59** (1987)

[7] R. Bulla, N. H. Tong, and M. Vojta, PRL **91**, 170601 (2003)

13 Gabriel Sellier:
Josephson Tunneling Through a Quantum Dot

Since its discovery [1] the Josephson effect has become one of the most important manifestations of superconductivity for technological applications and for various fields of research [2]. The issue of the present work is the investigation of the interplay between this remarkable effect and the interaction effects becoming apparent in quantum dots.

In his original work Josephson studied two superconductors separated by a tunnel-barrier. This barrier is assumed to be thin in order to allow the wave-functions in both superconductors to overlap. As soon as the symmetry between the phases of the wave-functions is broken, a charge current mediated by Cooper pairs (critical or Josephson current I_c) will flow through the junction, even without bias. In this limit where no transport voltage is applied, the critical current is given by the fundamental relation

$$I_c = I_{c0} \sin(\Phi_L - \Phi_R), \tag{1}$$

the $\Phi_{\alpha=L,R}$ are the phases in the corresponding left and right superconductor. The maximal current I_{c0} is positive and contains the microscopic details of the junction which will be referred to as a *0-junction* in the forthcomming context.

Since the pioneering work of Josephson various geometries have been investigated where the simple tunnel-barrier is replaced by different layers. Within the large number of systems studied the superconducting-ferromagnetic-superconducting junction (SFS) plays a prominent role. As a consequence of the ferromagnetic order parameter the Cooper pairs passing the SFS-junction accumulate an additional phase-shift leading for a certain thickness of the ferromagnetic layer to a change of sign in the maximal current I_{c0}. In this limit the Josephson junction is called a *π-junction*. Note that a transition between 0- and π-junction behavior (*0/π-transition*) is obtained, for instance, by simply varying the thickness of the ferromagnetic layer.

It is known that the a $0/\pi$-transition may also be observed in a system consisting of a quantum dot (QD) quenched between two superconductors [3]. In contrast to the SFS-junction the transition is solely controlled by the coupling strength between the QD and the superconductor. The mechanism for this transition is based upon interaction effects occurring in QDs when driven in the Coulomb blockade regime, where the number of electrons confined in the dot is quantized. If the dot is singly occupied (odd number of electrons) and the on-site repulsion becomes large preventing the dot to be populated with two electrons (even number of electrons), a local magnetic moment is formed (see figure 13a). For a Cooper pair tunneling across the junction this localized spin leads to a change in the spin ordering and to an additional minus sign in the maximal critical current I_{c0}. In this regime π-junction behavior is expected.

Alternatively, at low temperature conduction electrons tend to compensate the magnetic moment of the QD, a phenomenon well known as the Kondo effect [4]. In this case the localized spin is screened and the dot acts as a potential scatterer. Consequently, Cooper pairs crossing the junction do not experience a change in the spin ordering; we recover the signature of a 0-junction.

As the efficiency of the spin screening, which is provided by conduction electrons in a small region of width T_K around the Fermi surface (the Kondo temperature T_K is the characteristic energy scale dominating the Kondo effect), depends on the number of electronic states in this energy range, s-wave superconductivity implying a gap Δ in the density of states will strongly affect this phenomenon. Indeed, two interaction domains may be identified: (1) If $\Delta \gg T_K$ (weak coupling limit) the gap prevents spin compensation leading to π-junction behavior. (2) If $\Delta \ll T_K$ (strong coupling limit) the Kondo effect can fully develop and a 0-junction signature

is found.

We have investigated in detail the interplay between the two energy scales Δ and T_K within a self-consistent approximation and calculated the Josephson current through the system. In figure 13b the junction phase diagram is shown as a function of the interaction parameter T_K/Δ. The $T = 0$ value has been extrapolated which is found to be consistent with the value obtained from a poor-man's-scaling analysis.
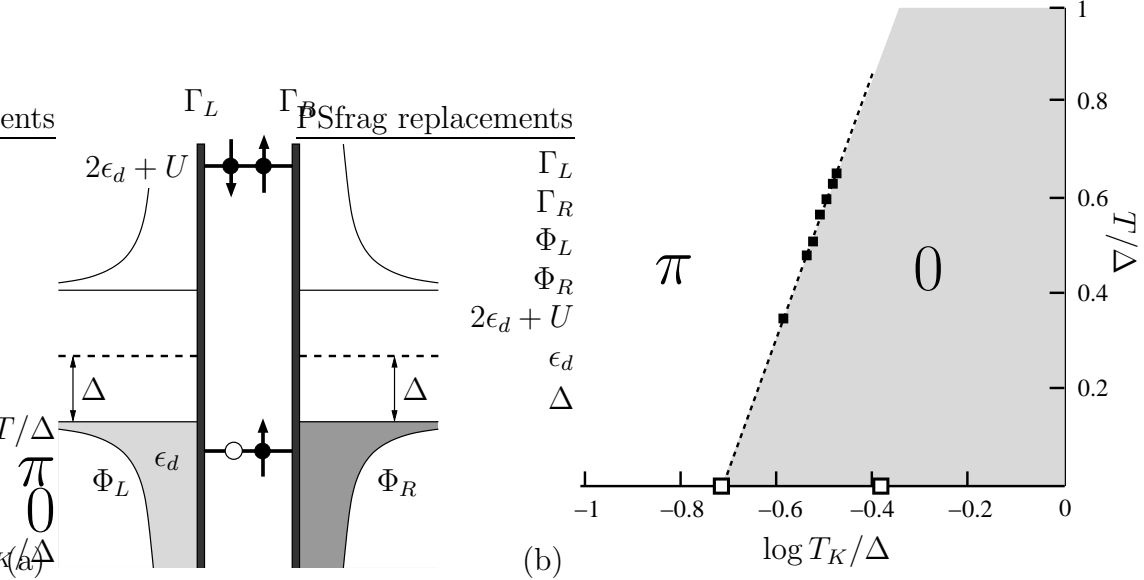
Figure 1: (a) Spectral representation of a QD coupled to two s-wave superconductors: Γ_L and Γ_R denote the effective couplings to the left and right lead. The singly occupied orbital has the energy ϵ_d. In the case of double occupancy this level is lifted up to $2\epsilon_d + U$ due to the Coulomb repulsion U. Φ_L and Φ_R label the phases of the left and right order parameter. The BCS gap Δ is assumed to be equal in both superconductors.

(b) Phase diagram of the junction as calculated within a self-consistent approach: For small coupling strengths ($T_K/\Delta \ll 1$) the junction exhibits a π-junction behavior due to dominant spin-scattering. On the other hand, in the strong coupling regime ($T_K/\Delta \gg 1$) the localized spin is compensated by conduction band electrons; the QD merely acts as a potential scatterer and a 0-junction signature is observed. At $T = 0$ the left square represents the extrapolated zero temperature result. The right square is calculated within an NRG-analysis [5] for a particle-hole symmetric spectrum of the dot.

[1] B. D. Josephson, *Phys. Lett.* **1**, 251 (1962)

[2] M. Tinkham, *Introduction to Superconductivity*, (McGraw-Hill, New-York, 1996)

[3] A. A. Clerk and V. Ambegaokar *Phys. Rev. B* **61**, 9109 (2000)

[4] A. C. Hewson, *The Kondo Problem to Heavy Fermions*, (Cambridge University Press, Cambridge, 1993)

[5] M. Choi, M. Lee, K. Kang, and W. Belzig, cond-mat/0312271

14 Dmitry Lobaskin:
Crossover from Non-Equilibrium to Equilibrium Behavior in the Time-Dependent Kondo Model

We investigate the equilibration of a Kondo model that is initially prepared in a non–equilibrium state towards its equilibrium behavior for large times. Such initial non–equilibrium states are, e.g., realized in quantum dot experiments with time–dependent gate voltages, or in rf SQUIDS. For that we use the following model which describes the interaction of a spin-1/2 degree of freedom $\vec{S}$ with a Fermi sea

$$H = \sum_{k\alpha} \varepsilon_k c_{k\alpha}^+ c_{k\alpha} + \sum_i J_i(t) \sum_{\alpha\beta} c_{0\alpha}^+ \vec{S}_i \cdot \vec{\sigma}_i^{\alpha\beta} c_{0\beta} \tag{1}$$

where we allow anisotropic scattering $J_i(t) = (J_\perp(t), J_\perp(t), J_\parallel(t))$. We investigate two types of non-equilibrium situations:

- I) the impurity spin is frozen for times $t < 0$ by, e.g., a large magnetic field term $h(t)S_z$ that is applied for $t < 0$ and switched off at $t = 0$:

$$h(t) = \begin{cases} h \gg J_i & , \; t < 0 \\ 0 & , \; t > 0 \end{cases}$$

- II) The impurity spin is decoupled from the bath degrees of freedom for times $t < 0$ and then the coupling is switched on at $t = 0$:

$$J_\parallel(t) = \begin{cases} 0 & , \; t < 0 \\ J_\parallel & , \; t > 0 \end{cases} \quad ; \quad J_\perp(t) = \begin{cases} 0 & , \; t < 0 \\ J_\perp & , \; t > 0 \end{cases}$$

There are few exact results for the time-dependent Kondo model. Several attempts were made to solve this problem numerically or semi-analytically in recent papers of Nordlander *et al.*[1] and Costi [2], where average impurity spin and spin-spin correlation functions were investigated:

$$P(t) \overset{\text{def}}{=} \langle S_z(t) \rangle$$

$$C(t, t_w) \overset{\text{def}}{=} \frac{1}{2} \langle \{S_z(t_w), S_z(t_w + t)\} \rangle \quad .$$

We evaluate the non–equilibrium spin–spin correlation function at the Toulouse point ($J_\parallel/2\pi v_F = 1 - 1/\sqrt{2}$) of the Kondo model exactly. To transform the Kondo Hamiltonian into an exactly solvable model we apply several steps: bosonization (to use spin-charge separation), unitary transformation (to remove the longitudinal coupling term) and refermionization (leading to fermionic degrees of freedom).

At the Toulouse point we get a quadratic (!) Hamiltonian. We diagonalize the Hamiltonian for $t < 0$ and $t > 0$ separately (expressed in terms of unperturbed Fermi sea operators), solve the Heisenberg equations of motion for operators for positive times, and take the average with respect to either I) or II) initial states (Fermi sea or potential scattering ground state). We show that there is a smooth crossover between non–equilibrium exponential and power-law

equilibrium behavior (see Leggett *et al.* [3]) as the non–equilibrium initial state evolves as a function of the waiting time for the first spin measurement. Our main result is

$$C_{I,II}(t_w, t) = \frac{1}{4}e^{-2t/t_K} - \left(s(t) - s(t_w + t)e^{-t_w/t_K} + s(t_w)e^{-(t_w+t)/t_K}\right)^2$$

with $s(t) = \int_0^\infty dx \frac{\sin(tx)}{x^2 + (1/t_K)^2}$. Notice that $s(t) \propto t^{-1}$ for $t \gg t_K$.

Away from the Toulouse point we use the flow equation method to solve the Heisenberg equations of motion by utilizing the mapping to an effective resonant level model with a nontrivial hybridization function $J_\perp \to J_\perp(k)$ [4]. Analytical and numerical results show the same universal features as at the Toulouse point:

- exponential decay of $P(t)$

- exponential approach to equilibrium

These results are depicted in Fig. 1.
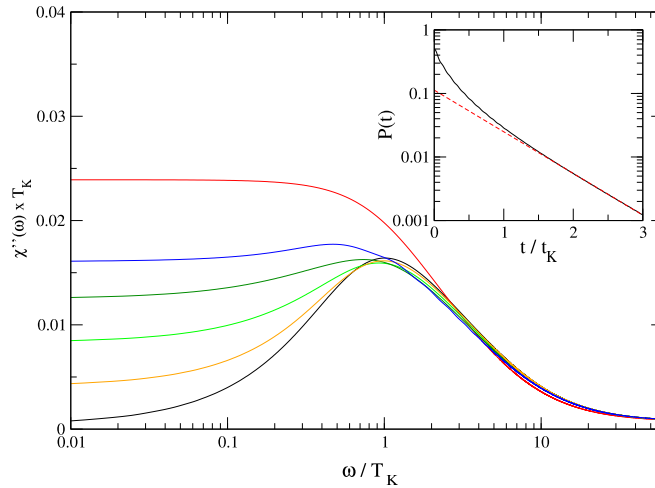
Figure 1: Universal curves for the dynamic spin susceptibility $\chi''(t_w, \omega)$ in the limit of small Kondo couplings (Kondo limit) for various waiting times ($t_w = 0, t_K/4, t_K/2, t_K, 2t_K, \infty$ from top to bottom). The inset shows the spin expectation value $P(t)$: the dashed line is an asymptotic fit $P_{\text{asym}}(t) = 0.11 \exp(-1.51\, t/t_K)$.

[1] P. Nordlander, M. Pustilnik, Y. Meir, N. S. Wingreen, and D. C. Langreth, Phys. Rev. Lett. **83**, 808 (1999); P. Nordlander, N. S. Wingreen, Y. Meir, and D. C. Langreth Phys. Rev. B **61**, 2146 (2000); M. Plihal, D. C. Langreth, and P. Nordlander, Phys. Rev. B **61**, R13341 (2000).

[2] T. Costi, Phys. Rev. B **55**, 3003 (1997).

[3] A. J. Leggett, S. Chakravarty, A. T. Dorsey, M. P. A. Fisher, A. Garg and W. Zwerger, Rev. Mod. Phys. **59**, 1 (1987).

[4] C. Slezak, S. Kehrein, Th. Pruschke, and M. Jarrell, Phys. Rev. B **67**, 184408 (2003).

15 Udo Schwingenschlögl:
Electronic Structure of Vanadium Oxides

In this talk the electronic structures and, in particular, the metal-insulator transitions (MITs) of a broad class of vanadium oxides are discussed in comparison to each other. The investigation is based on results from LDA electronic structure calculations, applying the augmented spherical wave (ASW) method [1, 2, 3].

Temperature induced MITs in transition metal oxides oftentimes coincide with characteristical structural transformations. In general, these compounds give rise to highly interesting physical phenomena because many of them are characterized by narrow metal d bands in the vicinity of the Fermi energy. As narrow d states are susceptible to electronic correlations, they are likely to show unusual electronic properties. In addition, the d states form directed bonds, which paves the way for strong electron-phonon coupling or degeneracy lifting processes as orbital ordering, for example. Since various mechanisms have to be considered, it is not surprising that in many cases controversial discussions concern the driving forces of the phase transitions.

In this context a large number of both experimental and theoretical investigations dealing with the MITs in the class of the vanadium oxides is reported in the literature. Special focus is on the prototypical compounds vanadium dioxide (VO_2) and sesquioxide (V_2O_3). However, much dispute remains concerning the origin of the phase transitions in the two materials. While it is agreed that they trace back to the delicate interplay of electron-phonon coupling and electronic correlations, the relative importance of these mechanisms is a matter of ongoing discussions.

For a deeper understanding of the transitions, an identification of the relevant electronic states and an investigation of their response to the changes of the crystal structure is desirable. This issue can be addressed by analyzing the relations between structural and electronic properties in the broader class of the vanadium Magnéli phases, which set up the homologous series V_nO_{2n-1} ($3 \leq n \leq 9$) and have crystal structures comprising typical dioxide and sesquioxide-like regions. The Magnéli phases are intermediate between the structures of the end members VO_2 ($n \rightarrow \infty$) and V_2O_3 ($n = 2$), which allows us to study the crossover between the latter oxides. Moreover, with only one exception, they exhibit MITs as a function of temperature. Since the transitions are accompanied by structural transformations, modifications of the local atomic environments can be related to the electronic behaviour.

Table 1 summarizes transition temperatures from electrical resistivity measurements. Moreover the table gives the formal V $3d$ valence charges of the vanadium Magnéli compounds, varying from two in V_2O_3 to one in VO_2.

Compound V_nO_{2n-1}	Parameter n	Formal V $3d$ charge	MIT temperature
V_2O_3	2	2	168 K
V_3O_5	3	$5/3 \approx 1.67$	430 K
V_4O_7	4	$6/4 \approx 1.50$	250 K
V_5O_9	5	$7/5 \approx 1.40$	135 K
V_6O_{11}	6	$8/6 \approx 1.33$	170 K
V_7O_{13}	7	$9/7 \approx 1.29$	metallic
V_8O_{15}	8	$10/8 \approx 1.25$	70 K
V_9O_{17}	9	$11/9 \approx 1.22$	—
VO_2	∞	1	340 K

Table 1: Formal V $3d$ charges as well as transition temperatures in the series V_nO_{2n-1}.
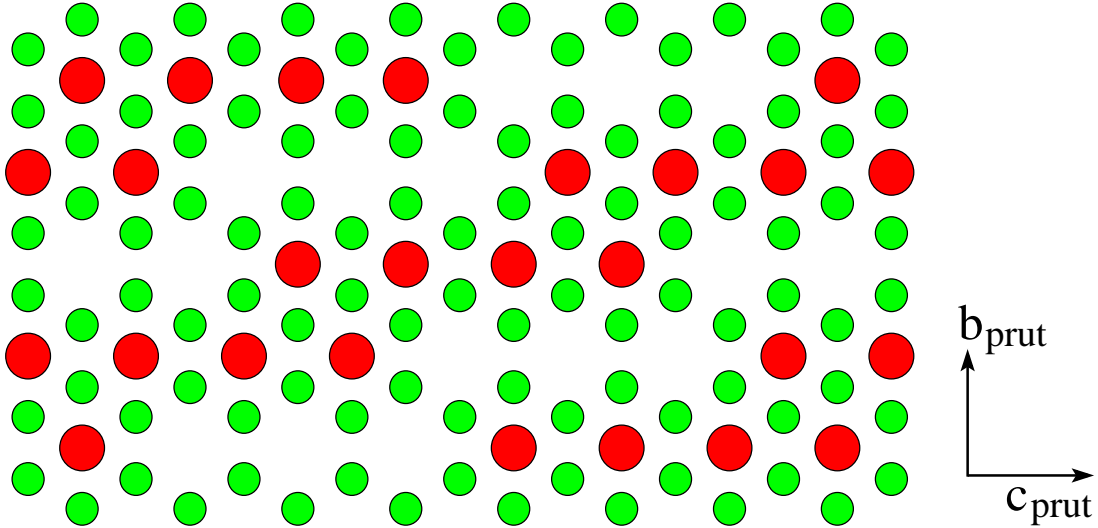
Figure 1: Crystal structure of V_4O_7: projection along a_{prut} of a O-V-O sandwich-like slab.

The crystal structures of the Magnéli phases are best described starting with the oxygen sublattice, which turns out to be similar for all compounds. The oxygen sites form a regular space filling network of neighbouring octahedra, which are mutually connected via edges in the c_{prut}-direction and via faces along both a_{prut} and b_{prut}. To illustrate the geometrical arrangement, a schematical projection along a_{prut} of a sandwich-like O-V-O slab from the crystal structure of V_4O_7 is displayed in figure 1. This slab consists of a vanadium layer confined by oxygen layers. Because of the projection, oxygen octahedra appear in the figure as hexagonal structures. We observe chains of vanadium atoms parallel to the c_{prut}-axis, comprising four metal sites in the case of V_4O_7. In general, the chains have length n for V_nO_{2n-1}. Therefore the Magnéli phases entail a systematic connection between the crystal structures of VO_2 and V_2O_3.

While V-O overlap places the V $3d$ t_{2g} states close to the Fermi energy, the detailed electronic structures and MITs of the Magnéli phases are essentially influenced by the local metal-metal coordination. The phase transitions arise as a result of electron lattice interaction in dioxide-like and electronic correlations in sesquioxide-like regions of the crystal structure. Dioxide-like metal atoms show the characteristical features of the embedded Peierls instability responsible for the MIT of VO_2. A combination of dimerization and antiferroelectric-like displacements of metal atoms by means of strong electron-lattice interaction causes splitting of the $d_{x^2-y^2} = d_\parallel$ states and energetical upshift of the d_{yz}/d_{xz} states. In contrast, vanadium atoms related to the sesquioxide are characterized by strongly reduced metal-metal overlap. As a consequence, the $d_{x^2-y^2}$ orbitals localize and the partial density of states resembles that of the d_{xz} orbitals. Due to the localization, electronic correlations may play an important role.

[1] U. Schwingenschlögl, V. Eyert, and U. Eckern, Europhys. Lett. **61**, 361 (2003); Europhys. Lett. **64**, 682 (2003).

[2] U. Schwingenschlögl, PhD-thesis, Universität Augsburg (2004).

[3] U. Schwingenschlögl and V. Eyert, Ann. Phys. (Leipzig), in press.

16   Georg Keller:
Realistic Modelling of Strongly Correlated Systems in LDA+DMFT

Conventional band structure calculations in the local density approximation (LDA) are highly successful for many materials but miss important aspects of the physics and energetics of strongly correlated electron systems, such as transition metal oxides and f-electron systems with Mott insulating and heavy quasiparticle behavior. In these systems, the LDA+DFMT scheme [1] has proved to yield valuable insights [2, 3, 4, 5]. LDA+DMFT does not only include the quasiparticle physics and the corresponding energetics but, at the same time, reproduces the LDA and LDA+U results in the limits where these methods are valid, see Figure 1.

Depending on the strength of the electronic correlation, a LDA+DMFT calculation yields the same weakly correlated result as the LDA, a strongly correlated metal, or a Mott insulator.

In the dynamical mean-field theory, the problem of electrons hopping on a lattice is mapped onto a self-consistent single impurity Anderson model, where the electrons interact on a single site and hybridize with the surrounding bath which is made of the same electrons. Therefore, two equations, one for the single impurity and one for the lattice (the Dyson equation) have to be solved iteratively, until self-consistency is reached. This is depicted in Fig. 2.

In its simplest form, strictly valid only for systems with degenerate bands, the LDA input to the DMFT calculations is the non-interacting density of states, which leads to the k-integrated Dyson equation

$$G_m(\omega) \;=\; \int d\epsilon \frac{N_m^0(\epsilon)}{\omega + \mu - \Sigma_m(\omega) - \epsilon}. \tag{1}$$

Here $G_m(\omega)$, $\Sigma_m(\omega)$, and $N_m^0(\omega)$ are the Green function, self energy, and LDA density of states, respectively, at energy ω for the t_{2g} orbital m.

Recently, the LDA+DMFT technique was extended to systems with non-degenerate bands. [6] Instead of the non-interacting LDA DOS, a reduced LDA Hamiltonian is used as input to
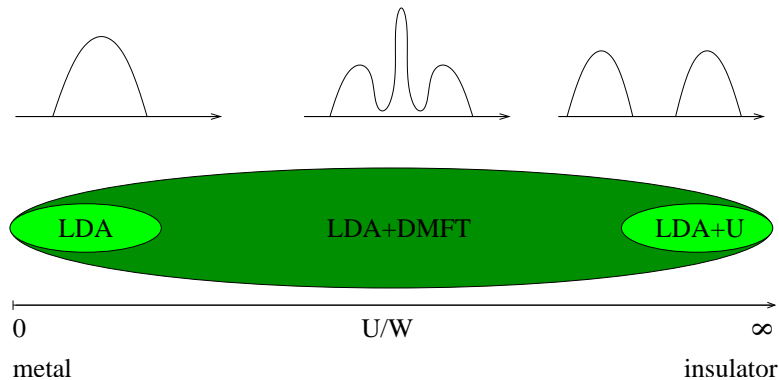
Figure 1: With increasing strength of the local Coulomb repulsion U (in comparison to the LDA band width W), one observes a weakly correlated metal (left density of states), a strongly correlated metal with a quasiparticle peak at the Fermi energy (middle) and a Mott insulator (right). The weakly correlated metal is correctly described by LDA and the energy of the (ordered) Mott insulator by LDA+U. LDA+DMFT gives the correct answer for all values of U and subsumes the LDA at small U/W and the LDA+U results for the Mott insulator occurring at large U/W.
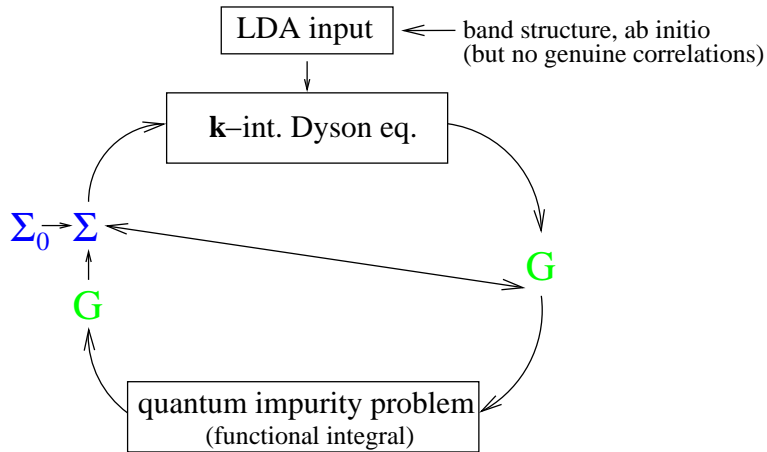
Figure 2: Calculation cycle of the LDA+DMFT

the DMFT-calculations, and the Dyson equation is extended to a k-integral over the first Brillouin zone. In the future, the goal is to advance the technique to a fully self consistent LDA+DMFT scheme, where the changes due to the DMFT calculations are fed back into the LDA calculations.

[1] K. Held, I. A. Nekrasov, G. Keller, V. Eyert, N. Blümer, A. K. McMahan, R. T. Scalettar, T. Pruschke, V. I. Anisimov, and D. Vollhardt *Realistic Investigations of correlated electron materials with LDA+DMFT* (Psi-k Newsletter No. 56 (April 2003), p. 65-103).

[2] K. Held, G. Keller, V. Eyert, D. Vollhardt, and V.I. Anisimov *Mott-Hubbard Metal-Insulator Transition in Paramagnetic V_2O_3: a LDA+DMFT(QMC) Study* (Phys. Rev. Lett. 86, 5345 (2001)).

[3] S.-K. Mo, J. D. Denlinger, H.-D. Kim, J.-H. Park, J. W. Allen, A. Sekiyama, A. Yamasaki, K. Kadono, S. Suga, Y. Saitoh, T. Muro, P. Metcalf, G. Keller, K. Held, V. Eyert, V. I. Anisimov, and D. Vollhardt *Prominent quasi-particle peak in the photoemission spectrum of the metallic phase of V_2O_3* (Phys. Rev. Lett. 90, 186403 (2003)).

[4] G. Keller, K. Held, V. Eyert, D. Vollhardt, V.I. Anisimov *Electronic Structure of Paramagnetic V_2O_3: Strongly Correlated Metallic and Mott Insulating Phase* (cond-mat/0402133).

[5] I.A. Nekrasov, Z.V. Pchelkina, G. Keller, Th. Pruschke, K.Held, A. Krimmel, D. Vollhardt, V.I. Anisimov *Orbital state and magnetic properties of LiV_2O_4* (Phys. Rev. B 67, 085111 (2003)).

[6] V.I. Anisimov, D.E. Kondakov, A.V. Kozhevnikov, I.A. Nekrasov, Z.V. Pchelkina, G. Keller, I. Leonov, X. Ren, D. Vollhardt, J.W. Allen, S.-K. Mo, H.-D. Kim, S. Suga, A. Sekiyama *Full orbital calculation scheme for electronic properties of strongly correlated systems* (in preparation).

17 Xinguo Ren: The Self-Consistent LDA+DMFT Scheme in Wannier Representation

The LDA+DMFT [1] method, which combines the density functional band calculation in local density approximation (LDA) and the many-body technique dynamical mean-field theory (DMFT), is a powerful tool to investigate real materials. However, the present scheme still needs to be improved. The reason is that so far it is carried out in a one-step way, i.e., the LDA band structure serves as the input information for a DMFT treatment, but there is no feedback from DMFT to LDA. On the other hand, the correlation effect introduced by DMFT could in principle change the charge distribution on which the LDA band structure itself depends. Thus, to make the whole scheme self-consistent, one needs to incorporate the changes of the charge density, and repeat the calculation until a convergence is reached.

The above appealing scheme was for a long time impeded by the misfit between the basis set used in LDA calculation and that in DMFT calculation. The Linear Muffin-Tin Orbitals (LMTOs) [2] basis is most widely used in the LDA band calculation, however it is not a good choice for solving the DMFT problem. First the width of the density of states (DOS) of LMTOs is usually very large; this makes a DMFT treatment difficult. Furthermore, LMTOs do not have integer fillings below the Fermi energy; but this is needed to obtain an insulating solution. Hence, before starting the DMFT calculation one has to cut the long tails of the LMTO DOS, renormalize it and then shift the Fermi energy to get an integer filling. This is awkward and causes uncontrollable errors. Most of all, this "operation" makes the feedback from DMFT to LDA unfeasible.

The abovementioned difficulties were recently solved by a new approach using Wannier function (WF) basis [3]. In this approach, a WF basis and a projected Hamiltonian are constructed by including the Bloch bands of interest at the Fermi level. Thus the energy window can be chosen freely and integer filling is also guaranteed. Furthermore, the transformation between a Wannier basis and a LMTO basis is well-defined, and therefore the self-energy given by the DMFT calculation in WF basis can be converted into the LMTO basis, so that the self-consistent loop is closed.

[1] V. I. Anisimov, A. I. Poteryaev, M. A. Korotin, A. O. Anokhin,and G. Kotliar, J. Phys. Cond. Matter **9**, 7359 (1997); K. Held, I.A. Nekrasov, G. Keller, V. Eyert, N. Blümer, A.K. McMahan, R.T. Scalettar, Th. Pruschke, V.I. Anisimov and D. Vollhardt, Psi-k Newsletter 56, 65 (2003) [psi-k.dl.ac.uk/newsletters/News_56/Highlight_56.pdf].

[2] O.K. Andersen, Phys. Rev. B **12**, 3060 (1975); O. Gunnarsson, O. Jepsen, and O.K. Andersen, Phys. Rev. B **27**, 7144 (1983).

[3] E. Pavarini, S. Biermann, A. Poteryaev, A. I. Lichtenstein, A. Georges, and O. K. Andersen, cond-mat/0309102; V. I. Anisimov, D. E. Kondakov, A. V. Kozhevnikov, I. A. Nekrasov, Z. V. Pchelkina, G. Keller, I. Leonov, X. Ren, D. Vollhardt, J. W. Allen, S.-K. Mo, H.-D. Kim, S. Suga, and A. Sekiyama, in preparation.

18 Torsten Rudolf: Optical Spectroscopy of Transition-Metal Oxides

Optical spectroscopy is the general term for a huge variety of experimental techniques, as for example laser resonance, laser modulation, raman and photoemission spectroscopy. Another method, called Fourier Transform Infrared (FTIR) Spectroscopy, is presented in this talk. Historically it all began with the discovery of the infrared radiation by Friedrich Wilhelm Herschel in the year 1800. [1] After the invention of the Bolometer detector and the Michelson interferometer in 1880, the first fully automated spectrometer was build in 1937 by BASF. But it was not until the mid-sixties that a new algorithm for Fourier transformations by Cooley and Tukey and fast computers made possible the Fourier Transform Spectroscopy as it is often used today. The most significant advantage of optical methods like the FTIR spectroscopy is, that the samples neither have to be destroyed nor contacted.

The frequency range which can be investigated by FTIR spectroscopy runs from about 20 to 40000 wavenumbers $[cm^{-1}]$ or 2 meV to 5 eV (1 eV $\approx$ 8000 cm^{-1}) in energy terms. It is divided into the far (FIR), middle (MIR), near infrared (NIR), and the visible (VIS) and ultraviolett (UV) region like it is shown in figure 1. Each region contains different physical
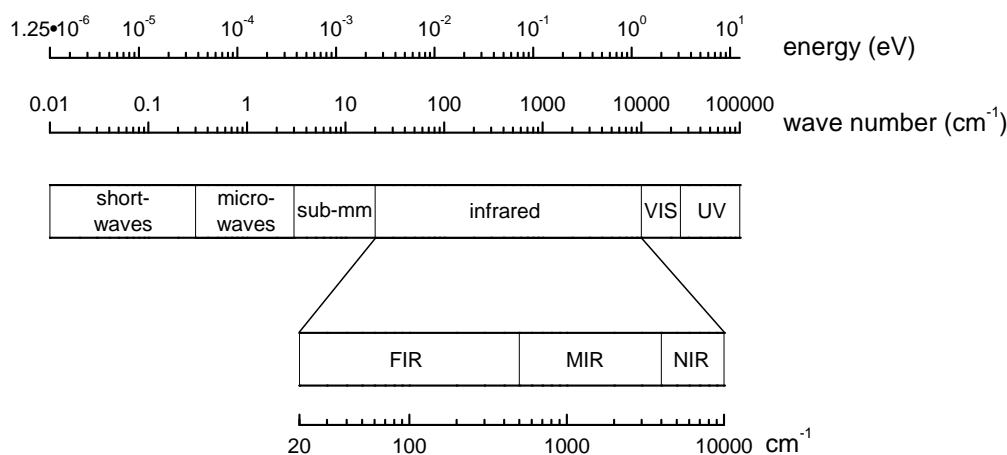
Figure 1: Division of the electromagnetic spectrum into different regions. The infrared section is further divided into far, middle and near infrared.

information: In the far infrared one can detect vibrational and rotational modes of gaseous molecules and phonon modes in solid states respectively. Observing a gas, the MIR provides information about vibrations of covalent bound molecules and especially group frequencies of organic functional groups. In a solid one can detect here polarons, but also intraband excitations and electronic (interband) transitions over band gaps. For higher frequencies, examination of gases show overtones and combinational vibrations of molecules in the NIR and absorption bands mainly of double bonds in the UV region respectively.
It is obvious that the FTIR spectroscopy with its huge information content is a popular technique not only for physical but also for chemical preparative and analytical research.

The fundamental condition for the possibility to detect vibrational transitions is either a static existent dipole moment or one which can be excited by the incident electromagnetic wave. This is why, for example, a vibrational mode, where in the linear CO_2 molecule the oxygen atoms

oscillate symmetrically towards the center C atom and back, cant't be seen in an infrared spectrum.

This talk gives information about the FTIR spectrometer, its buildup and the complex interplay of light sources, beamsplitters, windows, and detectors. Furthermore it is explained how the final transmission or reflection spectrum is obtained and how it is related with the optical constants absorption coefficient, conductivity and dielectric constant.
With results of measurements on $LaTiO_3$ as an example, interesting features in the reflectivity spectra are shown (see figure 2), concerning the phonon region as well as the domain of electronic transitions at higher energies.
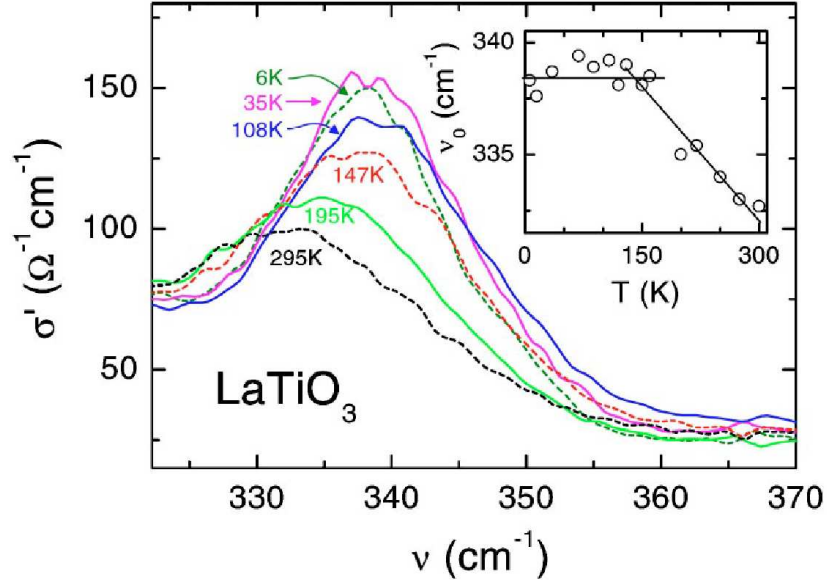
Figure 2: Anomaly in the phonon region of the reflectivity spectra of $LaTiO_3$. A sudden shift occurs at the magnetic ordering temperature T_N. [2]

In contrast, measurements on $Fe_{1-x}Cu_xCr_2S_4$ [3] for different doping levels exemplify the way electronic properties can be observed by FTIR spectroscopy and how they can be interpreted.

For further information on Fourier Transform Infrared Spectroscopy please see references [4] and [5].

[1] F. W. Herschel, Phil. Trans. Royal Soc. **90**, 284, 293, 437 (London, 1800)

[2] P. Lunkenheimer, T. Rudolf, J. Hemberger, A. Pimenov, S. Tachos, F. Lichtenberg, and A. Loidl, Phys. Rev. B. **68**, 245108 (2003)

[3] K. Pucher, T. Rudolf, F. Mayr, D. Samusi, V. Tsurkan, R. Tidecks, and A. Loidl, *Phonon anomalies and charge dynamics in $Fe_{1-x}Cu_xCr_2S_4$ single crystals*, submitted to Phys. Rev. B

[4] P. R. Griffiths, J. A. de Haseth, *Fourier Transform Infrared Spectrometry*, Wiley Interscience, New York, Chichester, Brisbane, Toronto, Singapore (1986)

[5] M. Dressel, G. Grüner, *Electrodynamics of Solids - Optical Properties of Electrons in Matter*, Cambridge University Press, Los Angeles (2002)

19   Markus Hoinkis:
Mott Transition at the Surface of *1T*-TaSe$_2$ Studied by Angle-Resolved Photoemission

The layered transition metal dichalcogenide *1T*-TaSe$_2$ is known to be in a charge density wave phase below $T_1 = 475K$. Recently, an additional phase transition occurring only at the *surface* has been discovered at $T_2 = 260K$ [1]. Below this temperature the density of states is strongly depressed at the Fermi energy.

The authors of [1] have interpreted this as a bandwidth-controlled Mott transition: The temperature-dependent modulation of the atomic positions leads to a smaller bandwidth W of the Ta 5d-Band. While this modification of the ratio U/W (U is the on-site Coulomb interaction) does not suffice to trigger a Mott transition in the bulk, the effective bandwidth at the surface could be sufficiently small for this effect.

Angle-resolved photoemission spectroscopy (ARPES) is an ideal tool to study this system:

- Since the mean free path of the photoelectrons is only a few monolayers, this method almost exclusively probes the surface.

- *1T*-TaSe$_2$ is a 2-dimensional system. It is well suited to investigate surface properties, because it can be easily cleaved in ultra-high vacuum. In this way, a clean surface can be revealed.

- The energy dispersion of *1T*-TaSe$_2$ is mainly within the plane parallel to the layers, because the overlap of the electrons' wavefunction between adjacent layers is negligible compared to the in-plane overlap. ARPES can map the energy dispersion along paths in k-space parallel to the sample's surface in a straightforward way. The reason for this is that the photoelectron's *parallel* momentum is conserved when leaving the crystal surface.

We have measured photoemission spectra to study the spectral evolution through the transition. Fig. 1 shows angle-integrated photoemission spectra above and below the transition. The intensity is proportional to the spectral function $A(E)$, which is the probability of removing an electron with the energy E from the N-electron system. In the case of a noninteracting electron gas, this would simply be the density of states. From the spectra one can see that the intensity at the Fermi energy E_F is suppressed when cooling below the transition temperature of 260K. This indicates that the sample surface turns from a metallic into an insulating state.
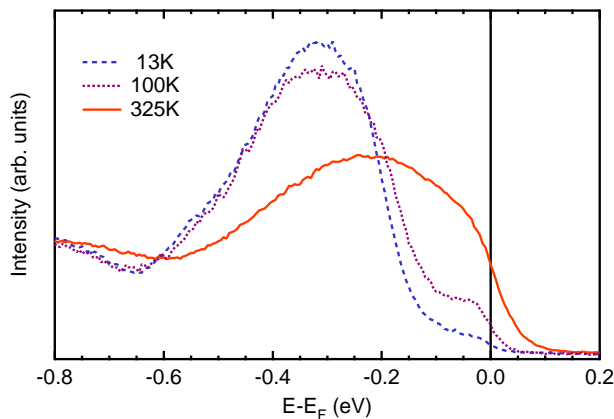
Figure 1: Angle-integrated photoemission spectrum of *1T*-TaSe$_2$

Fig. 2 displays ARPES intensity maps above and below the transition. Now, the spectral function $A(\mathbf{k}, E)$ not only depends on the energy E but also on the wavevector $\mathbf{k}$. The maps therefore directly show the energy dispersion of the valence band. Again, it can be clearly seen that below the transition spectral weight is removed from E_F, and a gap has appeared.
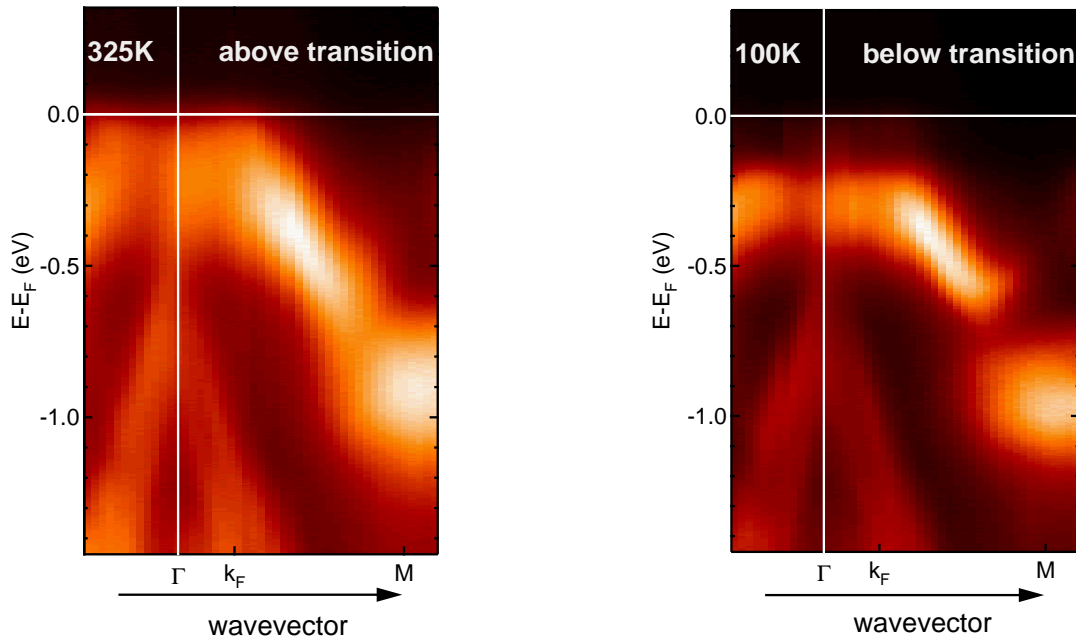
Figure 2: ARPES intensity maps of $1T$-TaSe$_2$ at T=325K (left) and T=100K (right) measured along the ΓM high-symmetry direction. Bright colors indicate high intensities.

It remains to be proven that a gap is opened everywhere on the Fermi surface, as it would be expected for a metal-insulator-transition. So far we have only shown this for selected regions in k-space. To this end further ARPES and scanning tunnelling spectroscopy (STS) experiments have to be conducted.

[1] L. Perfetti *et al.*, Phys. Rev. Lett. **90**, 166401 (2003).

List of Participants

Participant	Teilprojekt
Horacio Aliaga	B6
Cenap Ates	C6
Georg Eickerling	A2
Volker Eyert	A3
Robert Fichtl	C3
Thomas Götzfried	A1
Christian Helbig	A2
Markus Hoinkis	B3
Georg Keller	B6
Verena Körting	A4
Alexander Krimmel	B1
Christian Laschinger	B7
Hyun-Jung Lee	B5
Ivan Leonov	B6
Dmitry Lobaskin	B6
Robert Miller	A2
Carmen Mocanu	A3
Xinguo Ren	B6
Torsten Rudolf	C2
Daniela Schneider	C6
Udo Schwingenschlögl	A3
David Schrupp	B3
Gabriel Sellier	B7
Stefan Thiel	A4
Alexander Weber	A4

Acknowledgment